Master Thesis

Power Detector Second Order Correction Study applied to MIRAS/SMOS Mission

Author

Cristina González Haro

Department of Signal Theory and Communications
Universitat Politècnica de Catalunya (UPC)
C/Jordi Girona 1-3, D3-213, 08034 Barcelona (Spain)

SMOS Barcelona Expert Centre
Pg. Marítim de la Barceloneta, 37-49, 08003 Barcelona (Spain)
cristina.gonzalez@tsc.upc.edu

Thesis Advisors

Prof. Francesc Torres Torres
Prof. Núria Duffo Úbeda
[xtorres,duffo]@tsc.upc.edu
Department of Signal Theory and Communications
Universitat Politècnica de Catalunya (UPC)

Barcelona, February 2010

Acknowledgments

I would like to express my gratitude to Dr.Francesc Torres and Dr.Nuria Duffo, my thesis directors, for their support and suggestion during the performance of this thesis.

I want to express my gratitude in special manner to my office partner, Verónica González, who has provided assistance in numerous ways.

Thanks to MIER SA. Space Department for providing measurements data in which this thesis is based on.

I would like to thank Alan Tanner, from the Jet Propulsion Lab, Pasadena, for his valuable comments on the deflection method.

I would also like to thank my family, particular thanks to my parents. They have always supported and encouraged me to do my best in all matters of life.

And last but not least, I want to show my deepest gratitude to Ismael. He has made available his support in a number ways and always is besides me, specially at difficult times.

Contents

List of Figures

List of Tables

List of Acronyms

CAS	CAlibration Subsystem
CDTI	Centro para el Desarrollo Tecnológico Industrial
CMN	Control and Monitoring Node
CSIC	Consejo Superior Investigaciones Cientícas
DTS	Deflection Testing Software
ENR	Exces Noise Ratio
ESA	European Space Agency
FWF	Fringe Washing Function
IVT	Image Validation Tests
LICEF	LIghtweight Cost-Eective Front end
LSS	Large Space Simulator
MDB	MIRAS Data Base
MIRAS	Microwave Imaging Radiometer with Aperture Synthesis
MIRAS-TS	MIRAS Testing Software
NDN	Noise Distribution Network
NIR	Noise Injection Radiometer
PMS	Power Measurement System
SMOS	Soil Moisture Ocean Salinity
TVT	Thermal Vacumm Test
UPC	Universitat Politècnica de Catalunya

Chapter 1

Introduction

1.1 Scope of the thesis

The calibration of any Earth Observation sensor is a key stage which encompasses those tasks which are necessary to convert the raw measurement data into science data. The characterization of the instrument is a requirement for the development of the calibration activities. Characterization consists of the measurement of the typical behavior of instrument properties, including subsystems, which may affect the accuracy or quality of its response or derived data.

The scope of this master thesis is the characterization of non-linearity of the power detectors used to denormalize the digital correlations in interferometric radiometers, which may degrade the performance of the calibration procedures (image distortion).

This thesis has been mainly developed in the frame of projects devoted to assess and characterize the Microwave Imaging Radiomenter by Aperture Sythesis (MIRAS), the single payload of the European Space Agency (ESA) Soil Moisture and Ocean Salinity (SMOS) mission :

- 2008-2010: MIDAS-5. *"Microwave measurement analysis devoted to SMOS algorithm development"*. Ministerio de Educación y Ciencia Plan Nacional I+D+I ESP2007-65667-C04-02/FEDER (ongoing activities, SMOS Commissioning Phase preparatory work).
- 2007-2011: *"Specific collaboration agreement between the Universitat Politècnica de Catalunya and the Consejo Superior de Investigaciones Científicas to found the SMOS-Barcelona Expert Centre on Radiometric Calibration and Ocean Salinity (SMOS-BEC)"*. UPC and CSIC Consejo (Superior Investigaciones Cientícas)-Instituto de Ciencias del Mar (ongoing activities, SMOS Commissioning Phase preparatory work).

1.2 Objectives of the thesis

This thesis presents a comprehensive analysis of the impact of detector non-linearity and related correction techniques in the performance of the MIRAS instrument, which is the single payload of the European Space Agency (ESA) Soil Moisture and Ocean Salinity (SMOS).

Two different methods, the so-called Slope method and Deflection method have been developed and fully analyzed in order to characterize the non-linearities of the detectors first and finally to correct them. This study is focused to assess the best procedure to correct the non-linear response of the detectors, in the frame of calibration procedures of the SMOS mission.

1.3 Organization of the thesis

This section is devoted to describe the thesis organization, which is divided into eight chapters. The first chapters are devoted to introduce the reader in the context of the SMOS mission, as well as to give a general description of the instrument and the basic concepts of amplitude calibration. The following chapters present two different calibration methods in order to measure and correct the non-linearity of the power detector: the Slope method and the Deflection method. The two methods are analyzed in a similar way. First the characterization of the non-linearity and the correction technique are shown, to follow with the study of measurement uncertainty.

In this sense, Chapter 2 gives an overview of the SMOS mission and the instrument, in order to describe the context in which this thesis has been carried out.

Chapter 3 describes the amplitude calibration approach, and shows the need for non-linearity correction.

Chapter 4 shows the measurement test set-up calibration, and describes the measurement data set that are used in the performance analysis of the two calibration methods.

Chapters 5 and 6 give a comprehensive description of the Slope Method and the Deflection method respectivelly. As it has been said before, both chapters have the same structure. First the characterization of the non-linearity and the correction technique are described, to follow with a study of measurement uncertainty is performed.

Chapter 7 asseses the two non linearity correction procedures with relation to the MIRAS amplitude calibration requirements.

Finally, chapter 8 summarizes the mean conclusions of this work. This is completed by the list of publications as presented in appendix A.

Chapter 2

The SMOS mission

SMOS, acronym for Soil Moisture and Ocean Salinity, is an ESA Explorer Opportunity science mission, a technology demonstration satellite project in ESA's Living Planet Program, in cooperation with Centre National d'Etudes Spatiales (CNES) in France and the Centro para el Desarrollo Tecnológico Industrial (CDTI) (Center for Technological and Industrial Development) in Spain [1].

Known as ESA's 'Water Mission', SMOS has been designed to observe Soil Moisture [2] over the Earth's landmasses and Ocean Salinity [3] over the oceans for a period of at least 3 years. The observation of these two geophysical parameters will improve our understanding of Earth's water cycle, providing data useful for weather and climate models. [4]

The mission is comprised of a satellite in a low sun synchronous orbit, with an altitude of 755 Km and a revisit time of 3 days, that passively measures the electromagnetic noise generated by Earth at L-band (1.4 GHz) with a spatial resolution of 50-100 Km and radiometric sensitivity of 5K, in addition to a ground operations segment for the control and processing of data. The satellite was succesfully launched on 2nd November 2009 and at the moment of writting this thesis, it is on its Commissioning Phase.

Another important aspect of this mission is that it will demonstrate a new measuring technique. SMOS will carry the first-ever polarorbiting satellite-borne 2-D interferometric radiometer, the Microwave Imaging Radiometer with Aperture Sythesis (MIRAS) [5], [6], [7], which has been designed as a two-dimensional interferometer, which acquires brightness temperatures at L-band (1.4 GHz). Therefore, this mission will not only contribute to the understanding of the climate but it will also demonstrate a new techonology.

2.1 Scientific objectives

The main scientific objective of the SMOS mission is to provide global maps of Ocean Surface Salinity over oceans and Soil Moisture over land to advance climatologic, meteorologic, hydrologic, and oceanographic applications.

Measuring Soil Moisture means measuring the amount of water within a given volume of material and is usually expressed as a percentage. From space, the SMOS instrument can measure as little as 4% moisture in soil on the surface of the Earth - which is about the same as being able to detect less than one teaspoonful of water mixed into a handful of dry soil.

Parameter	Accuracy	Spatial Resolution	Revisit Time
Soil Moisture	$0.04\,m^3m^{-3}$ 4 %	$< 50\,Km$	$\leq 3\,days$
Ocean Salinity	$0.2 - 0.1\,psu$	$200 - 100\,Km$	$10 - 30\,days$

Table 2.1: The primary SMOS mission requirements for soil moisture and ocean salinity

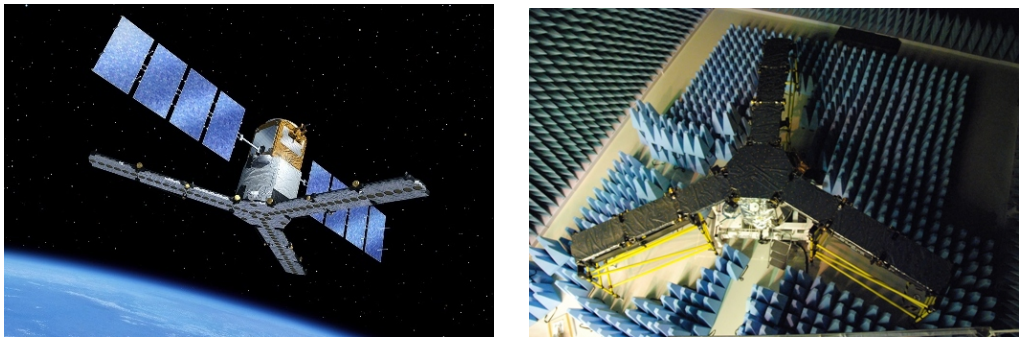

(a) Artistic view of MIRAS (b) MIRAS at Maxwell anechoic chamber

Figure 2.1: The MIRAS payload

While Salinity describes the concentration of dissolved salts in water. It measures in practical salinity units (psu), which expresses a conductivity ratio. The average salinity of the oceans is 35 psu, which is equivalent to 35 grams of salt in 1 litre of water. SMOS aims to observe salinty down to 0.1 psu (averaged over 10-30 days and an area of 200 km x 200 km) - which is about the same as detecting 0.1 gram of salt in a litre of water.

2.2 The SMOS payload: MIRAS

The single payload of the mission is the Microwave Imaging Radiometer with Aperture Synthesis (MIRAS). Its operating principle is based on a totally new technique for space-borne Earth observation: 2-D interferometric aperture synthesis. In order to achieve the required spatial resolution at this frequency band (1.4 GHz), a too large antenna would normally be necessary, using real aperture techniques. For the SMOS mission, however, the antenna aperture has been synthesized through a multitude of small antennae.

MIRAS instrument consists of a Y-shape synthetic aperture radiometer operating at L-band formed by 72 receivers called LICEFs (LIghtweight Cost-Eective Front end), equally distributed along the three deployable arms, which are connected to a central structure called hub. Each arm is divided into three segments, containing 6 receivers per segment. Three Noise Injection Radiometer (NIR) receivers have been included in the central hub. Each NIR comprises two LICEF receivers connected to a single antenna, thus the instrument is composed of 72 receivers but only 69 antennas. Each segment contains a Control and Monitoring Node (CMN) that provides power and a phased local oscillator to each LICEF.

Each LICEF is an antenna-received integrated unit that measures the radiation emit-

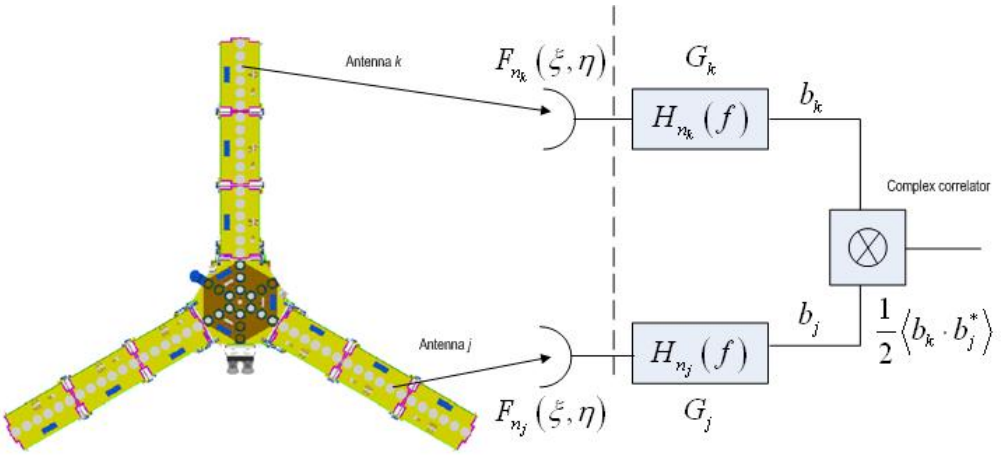

Figure 2.2: Block diagram of a single baseline relating the measurement of a sample of the visibility fuction.

ted from the Earth at L-band (1.4 GHz). The acquired signal is then transmitted to a central correlator unit, which performs interferometry cross-correlations of the signals between all possible combinations of receiver pairs (so-called baselines), providing the samples of the so-called visibility function [8]:

$$V_{kj}(u,v) = \frac{1}{k_B\sqrt{B_k B_j}\sqrt{G_k G_j}} \cdot \frac{1}{2} < b_k \cdot b_j^* > \tag{2.1}$$

where (u,v) correspond to the set of spatial frequencies where the visibility function is sampled (antenna separation in wavelengths), G_k, G_j are the power gains of each receiver chain and B_k, B_j correspond to the equivalent noise bandwiths.

One of the main differences between real aperture and interferometric radiometers is that the interferometric radiometers give a multipixel image after a Fourier Transform of the visibility function. It is, the interferometric radiometer does not perform a direct measurement of the brightness temperature but of a set of samples of its Fourier Transform. The following expression shows the visibility function of any pair of receivers k and j in terms of the brightness temperature:

$$V_{kj}(u,v) = \iint\limits_{\xi^2+\eta^2\leq 1} \frac{T_B(\xi,\eta)-T_r}{\sqrt{1-\xi^2-\eta^2}} \cdot \frac{F_{n_k}(\xi,\eta)\cdot F_{n_j}^*(\xi,\eta)}{\sqrt{\Omega_k\Omega_j}} \cdot \bar{\bar{r}}_{kj}\left(\frac{-u\xi+v\eta}{f_0}\right) \cdot e^{-j2\pi(u\xi+v\eta)} d\xi d\eta \tag{2.2}$$

where $\bar{r}_{kj}()$ corresponds to the Fringe Washing function normalized to unity at origin and it is related to the spatial decorrelation errors, $T_B(\xi,\eta)$ is the brightness temperature, $F_{n_k}(\xi,\eta)$, $F_{n_j}(\xi,\eta)$ are the normalized voltage antenna patterns, Ω_k, Ω_j correspond to the equivalent solid angle of the antennas, and (ξ,η) are the director cosines with respect to X and Y axes, respectively.

The calibrated visibility samples are inverted by the image reconstruction algorithm to get the brightness temperature maps as a function of the director cosines at the antenna reference plane. In a first approach, (identical antenna patterns, negligible spatial

decorrealation and no antenna positioning errors), this image reconstruction algorithm is performed by an inverse Fourier transform:

$$V_{kj}(u,v) = F\left[T_B(\xi,\eta)\right] \tag{2.3}$$

2.2.1 MIRAS calibration fundamentals

End-to-end calibration of MIRAS radiometer [9] refers to processing the measured raw data up to brightness temperature maps over the Earth's surface. The procedure starts with a self-correction of comparators offset and quadrature errors and it is followed by the calibration procedure itself. Regarding the calibration procedure, it is based on the injection of correlated and uncorrelated noise in the receivers and post-procesessing on ground the correlation results. The theoretical behind the concept was established in [10]. A noise distribution network called the calibration subsystem (CAS) [11] is applied to calibrate the receiver noise temperature and the relative phase characteristics of the receivers that compouned MIRAS. Some ancilliary data of different subsystems (such as relative S-parameters of the CAS and of the input switch), that are measured on ground by the different manufacturers, are required for the calibration procedure. While the whole process is independent of the exact value of the noise source power and of the noise distribution network (NDN) physical temperature. However, the approach relies on having at least one very well-calibrated reference receiver, which is implemented as a Noise Injection Radiometer (NIR) [12].

The detailed procedure, step by step calibration equations and correction techniques are included in [9] , [13] furthermore first results of the evalution of these procedures in the fully intagrated instrument can be found in [14].

Figure 2.3 shows a detailed block diagram of a baseline, which consists in two LICEF receivers and the complex 1-bit correlator. Moreover it includes the reference radiometer (NIR) and the different planes where the calibration equations are defined.

In summary the visibility samples can be denormalized and corrected from instrumental errors according the following expression:

$$V_{kj}^A = \frac{\sqrt{T_{sysk}^A T_{sysj}^A}}{G_{kj}^A} \cdot M_{kj} = H_{kj} \cdot M_{kj} \cdot e^{j\phi_{kj}} \tag{2.4}$$

where M_{kj} is the normalized complex correlations computed from the correlatons counts after the self-calibration procedure. T_{sysk}^A and T_{sysj}^A are the sysstem temperature referred to the antenna plane of LICEF k and LICEF j, respectively. G_{kj}^A is the Fringe Wash function term referred to the antenna plane.

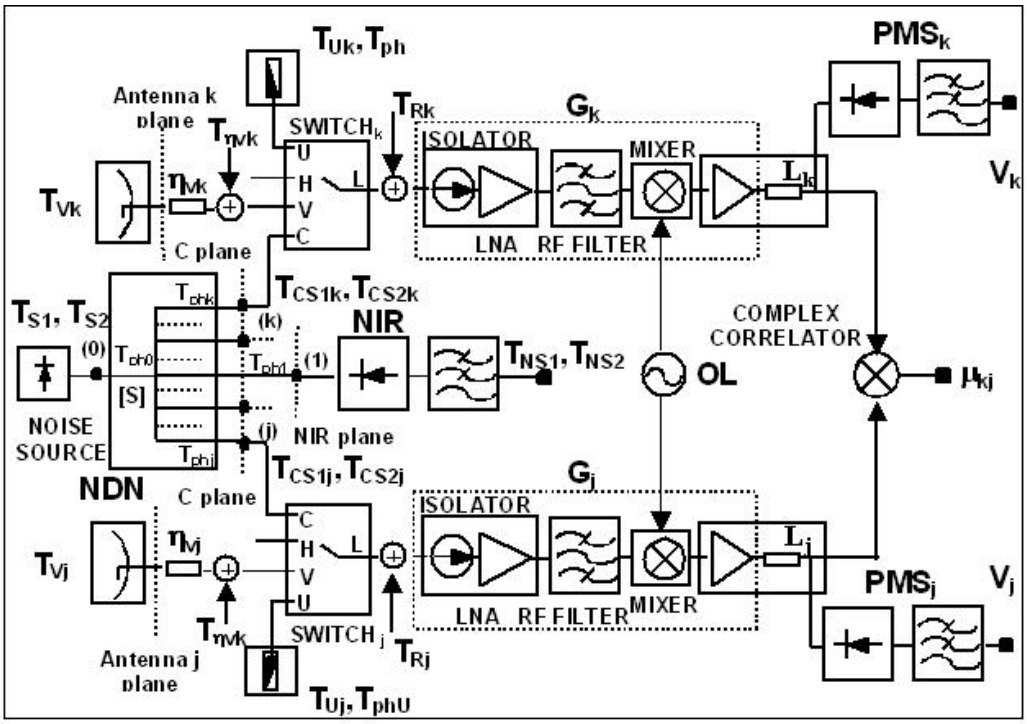

Figure 2.3: Block diagram of a single baseline, which consists in two LICEF units and a complex 1-bit correlator.

Chapter 3

The amplitude calibration

The amplitude calibration consists of estimating the unkonwn parameter H_{kj} in expression (2.4), which includes the system temperatures and the non-separable amplitude term. Both are determined by different procedures:

- T^A_{sysk} and T^A_{sysj} are the global system temperature measured at system input of receivers k, j. They are measured by means of a Power Measurement System (PMS) placed at each LICEF receiver. The PMS provides a voltage signal proportional to the input noise, and it must be either on-ground or in-orbit calibrated. This calibration method uses the two-level four-point method, that will be envisaged in section 3.1.
- $\left|G^A_{kj}\right|$ is the modulus of the fringe-washing term evaluated at the origin, where it has been assumed that the modulus of the fringe-wash term is the same for the (ii) and (qi) paths. It is measured by means of the correlated noise injection.

3.1 The four-point measurement technique

This technique as proposed in [15] is based on a linear model of the PMS. Hence, the measured voltage out of the PMS, v_{PMS}, when an equivalent system temperature T_{sys} is present at system input, is given by

$$v_{PMS} = v_{off} + GT_{sys} \tag{3.1}$$

where T_{sys} can be split into two terms relating the equivalent system noise temperature T_r, and the external temperature to be characterized T_{ext}:

$$T_{sys} = T_{ext} + T_r \tag{3.2}$$

The PMS is calibrated once the unknown parameters v_{off}, G and T_r are estimated. If the desired magnitude to be estimated is T_{sys}, then only v_{off} and G are required:

$$T_{sys} = \frac{v_{PMS} - v_{off}}{G} \tag{3.3}$$

Note that in such cases where only differential knowledge of T_{ext} is required, the T_r term is irrelevant since $T_{sys2} - T_{sys1} = T_{ext2} - T_{ext1}$. Now, let's have two known

external temperatures T_{C1} and T_{C2} where $T_{C1} < T_{C2}$. Hence T_{C1} is the so-called WARM temperature and T_{C2} the so-called HOT temperature. Now the overall system gain can be switched between two values G and G/L by means of a suitable attenuator placed in the signal path at a point that it can be considered noiseless (Figure 2.3). Then, the four voltage measurements out of the PMS are given by the following set of equations:

$$\begin{array}{c} v_1 = v_{off} + G(T_{C1} + T_r)\ PMS\,output\,WARM\,noise\,source = ON\,and\,L = OFF \\ v_2 = v_{off} + G(T_{C2} + T_r)\ PMS\,output\,HOT\,noise\,source = ON\,and\,L = OFF \\ v_3 = v_{off} + \frac{G}{L}(T_{C1} + T_r)\ PMS\,output\,WARM\,noise\,source = ON\,and\,L = ON \\ v_4 = v_{off} + \frac{G}{L}(T_{C2} + T_r)\ PMS\,output\,HOT\,noise\,source = ON\,and\,L = ON \end{array} \tag{3.4}$$

The desired parameters can be readily obtained as

$$v_{off} = \frac{v_2 v_3 - v_1 v_4}{(v_2 - v_4) - (v_1 - v_3)} \quad and \quad G = \frac{v_2 - v_1}{T_{C2} - T_{C1}} \tag{3.5}$$

and the estimated system temperature is obtained through

$$T_{sys} = \frac{v - v_{off}}{v_2 - v_1}(T_{C2} - T_{C1}) \tag{3.6}$$

It is worth to notting that a major advantage of this method is that only the differential value of T_{C1} and T_{C2} is required. Also note that actual value of the attenuator, L, is not required. However, it has a large impact in the estimation of v_{off}, since the values into parenthesis in expression (3.5) tend to zero as L tends to 1 (0 dB).

Now, relating calibration of the PMS within each LICEF unit, it has been proposed up to now to use the U source (matched load) to implement the low level noise source T_{C1} and the C source (correlated noise source) to implement the HOT noise source T_{C2}. In this sense, T_{C1}can be written as:

$$T_{C1} = T_U + \Delta T_U \tag{3.7}$$

where T_U is the physical temperature of the matched load at the T_U port and ΔT_U a bias that depends on the return loss of the matched load and the ohmic losses of the connection path to the U port of the switch.

The HOT temperature is injected through the noise distribution network (NDN) to the C port of the switch. It can be expressed as:

$$T_{C2} = T_S \left|S_{ko}\right|^2 + \Delta T_{[S],T_{ph}} \tag{3.8}$$

Where T_S is the temperature of the HOT noise source, connected to the port "0" of the NDN and S_{k0} is the S-parameter from the noise source and the "k" port of the NDN (receiver "k" has been considered). The term $\Delta T_{[S],T_{ph}}$ stands for the error contribution of the NDN itself. It depends on its physical temperature and the uncertainty in the measurement of its S-parameters.

At this point, the system temperature can be written as:

$$T_{sys} = \frac{v - v_{off}}{v_2 - v_1}(T_S \left|S_{k0}\right|^2 - T_U + \Delta T_{[S],T_{ph}} - \Delta T_U) \tag{3.9}$$

As it is readily seen, since uncertainties in the HOT and WARM measurements are independent they will add in a quadratic sense. Moreover, the uncertainty in the measurement of the HOT temperature is very large due to the noise contribution of the NDN itself that cannot be neglected. In order to remove this contribution, absolute measurement of the NDN S-parameters would also be required.

Hence, in order to eliminate systematic errors and the noise contribution of the NDN, the next section proposes to perform a relative amplitude calibration approach.

3.2 Relative amplitude calibration approach

This section shows a relative amplitude calibration approach that eliminates systematic errors and the noise contribution of the NDN.

Figure 2.3 shows a simplified block diagram to illustrate the relative amplitude calibration approach. As shown, both the HOT and the WARM temperatures are synthesized by the common external noise source and injected to each LICEF through the noise distribution network (NDN). That means that two equivalent noise temperatures T_{S1} (WARM) and T_{S2} (HOT) are delivered to the port "0" of the NDN (Figure 2.3). These temperatures are measured by the NIR, giving the equivalent external temperatures at NIR plane T_{NS1} and T_{NS2} (port "1" of the NDN). The equivalent external temperatures at the calibration plane of the LICEF units (ports "k" and "j" of the NDN) are T_{CS2k}, T_{CS2j}, T_{CS1k} and T_{CS1j}. However, it must be taken into account that the NDN is a lossy network which introduces additional temperature terms related to its physical temperature. For instance, from eq.44 chap 3 of [16], the equivalent temperatures at ports "1" and "k" of the NDN when the HOT temperature is injected by the noise source are given by:

$$\begin{aligned} T_{CS2k} &= T_{S2}\left|S_{k0}\right|^2 + \Delta T_{[S],T_{ph}} \\ T_{NS2} &= T_{S2}\left|S_{10}\right|^2 + \Delta T'_{[S],T_{ph}} \end{aligned} \tag{3.10}$$

Where the ΔT and $\Delta T'$terms include the contribution of the NDN due to its physical temperature.

Now, we can write T_{CS2k} and T_{CS1k} as a function of the temperatures measured by the NIR.

$$\begin{aligned} T_{CS2k} &= \frac{T_{NS2}-\Delta T'_{[S],T_{ph}}}{\left|S_{10}\right|^2}\left|S_{k0}\right|^2 + \Delta T_{[S],T_{ph}} \\ T_{CS1k} &= \frac{T_{NS1}-\Delta T'_{[S],T_{ph}}}{\left|S_{10}\right|^2}\left|S_{k0}\right|^2 + \Delta T_{[S],T_{ph}} \end{aligned} \tag{3.11}$$

Introducing these expressions into (3.6), the system temperature for receiver k can be rewritten eliminating its dependence with the physical temperature

$$T_{sysk} = \frac{v - v_{off}}{v_2 - v_1}\frac{\left|S_{k0}\right|^2}{\left|S_{10}\right|^2}(T_{NS2} - T_{NS1}) \tag{3.12}$$

It must be pointed out that T_{sysk} derived from 3.9 gives the equivalent system temperature at plane C, no matter where it has been originated. To make this explicit we will write T^C_{sysk} as system equivalent noise at the calibration plane ("k" port of the NDN).

$$T^C_{sysk} = \frac{v - v_{off}}{v_2 - v_1} \frac{|S_{k0}|^2}{|S_{10}|^2} (T_{NS2} - T_{NS1}) \tag{3.13}$$

Now, if we desire to know the equivalent system temperature at the antenna plane T^A_{sysk} in figure 2.3 (T^H_{sysk} for the horizontal mode and T^V_{sysk} for the vertical mode), then a plane transformation must be performed, taking into account that

$$T^H_{sysk} = T^C_{sysk} \frac{|S_{LC}|^2}{|S_{LH_k}|^2 \eta_{H_k}} \tag{3.14}$$

substituing expression (3.13)in (3.14):

$$T^H_{sysk} = \frac{v^H_k - v_{off_k}}{v_{2_k} - v_{1_k}} \frac{|S_{k0}|^2}{|S_{10}|^2} \frac{|S_{LC_k}|^2}{|S_{LH_k}|^2 \eta_{H_k}} (T_{NS2} - T_{NS1}) \tag{3.15}$$

Where $|S_{LC_k}|$ and $|S_{LH_k}|$are the modulus of the switch S-parameters relating ports C and H with port L in receiver k (Figure 2.3). η_{H_K} is the ohmic efficiency of antenna k in H mode.

The same procedure can be applied to receiver j

$$T^H_{sysj} = \frac{v^H_j - v_{off_j}}{v_{2_j} - v_{1_j}} \frac{|S_{j0}|^2}{|S_{10}|^2} \frac{|S_{LC_j}|^2}{|S_{LH_j}|^2 \eta_{H_j}} (T_{NS2} - T_{NS1}) \tag{3.16}$$

and the amplitude calibration term H_{kj} in (2.4) can be rewritten as

$$H^H_{kj} = \frac{1}{|G^H_{kj}|} \sqrt{\frac{v^H_k - v_{off_k}}{v_{2_k} - v_{1_k}} \frac{v^H_j - v_{off_j}}{v_{2_j} - v_{1_j}}} \frac{|S_{k0}| |S_{j0}|}{|S_{10}|^2} \frac{|S_{LC_k}|}{|S_{LH_k}|} \frac{|S_{LC_j}|}{|S_{LH_j}|} \frac{(T_{NS2} - T_{NS1})}{\sqrt{\eta_{H_k} \eta_{H_j}}} \tag{3.17}$$

At this point, we can make explicit that the calibration amplitude term is different for the horizontal and vertical measurement modes:

$$H^V_{kj} = \frac{1}{|G^V_{kj}|} \sqrt{\frac{v^V_k - v_{off_k}}{v_{2_k} - v_{1_k}} \frac{v^V_j - v_{off_j}}{v_{2_j} - v_{1_j}}} \frac{|S_{k0}| |S_{j0}|}{|S_{10}|^2} \frac{|S_{LC_k}|}{|S_{LV_k}|} \frac{|S_{LC_j}|}{|S_{LV_j}|} \frac{(T_{NS2} - T_{NS1})}{\sqrt{\eta_{V_k} \eta_{V_j}}} \tag{3.18}$$

where v^H_k and v^V_k are the PMS voltage readings when the switch of the LICEF "k" is in the H and V positions respectively. Now the only unknown is the fringe-washing term G_{kj}.

The next section shows the estimation of the fringe-washing term G_{kj}.

3.3 Estimation of the fringe-washing amplitude term

When a single source is used to inject noise simultaneously to a set of receivers, such as the hub or each one of the sections, the complex cross-correlation of a given baseline depends on the difference between the noise temperature of the source T_S and the physical

temperature of the network T_{ph} [16]. In particular, assuming certain approximations discussed in chapter 3 of the mentioned reference, (2.4) can be written as:

$$S_{k0}S_{j0}^{*}\left(T_S - T_{ph}\right) = H_{kj}^{C}M_{kj}^{C}e^{j\alpha_{kj}} \tag{3.19}$$

In principle, the fringe-washing amplitude term need not be explicitly estimated. In fact, by dividing (2.4) by and taking into account the definition of amplitude calibration H_{kj} (2.4), the following compact expression for the corrected visibility is obtained:

$$\hat{V}_{kj} = S_{k0}S_{j0}^{*}\left(T_S - T_{ph}\right)\frac{\sqrt{T_{sys_k}T_{sys_j}}}{\sqrt{T_{sys_k}^{C}T_{sys_j}^{C}}}\frac{M_{kj}}{M_{kj}^{C}} \tag{3.20}$$

where T_{sys_k} is measured at the antenna plane of receiver "k" and $T_{sys_k}^{C}$ is measured at its calibration plane C (port "k" of the NDN in Figure 2.3).

Although, while this equation is useful to obtain the phase of the corrected visibility, its direct application to infer its amplitude relies on the knowledge of the absolute modulus of the S-parameters and of the physical temperature distribution throughout the system.

A very robust estimation of G_{kj} can be obtained, performing two measurements at two different correlated temperatures T_{S1} and T_{S2}. The modulus of (3.19), evaluated at T_{S1} and T_{S2} can be written as:

$$\begin{aligned}\tfrac{1}{G_{kj}}\sqrt{T_{sys_k}^{C1}T_{sys_j}^{C1}}\left|M_{kj}^{C1}\right| &= \left|S_{k0}\right|\left|S_{j0}\right|\left(T_{S1} - T_{ph}\right)\\ \tfrac{1}{G_{kj}}\sqrt{T_{sys_k}^{C2}T_{sys_j}^{C2}}\left|M_{kj}^{C2}\right| &= \left|S_{k0}\right|\left|S_{j0}\right|\left(T_{S2} - T_{ph}\right)\end{aligned} \tag{3.21}$$

Now, subtracting one equation from the other and arranging terms, the fringe-washing term is obtained

$$G_{kj} = \frac{\sqrt{T_{sys_k}^{C2}T_{sys_j}^{C2}}\left|M_{kj}^{C2}\right| - \sqrt{T_{sys_k}^{C1}T_{sys_j}^{C1}}\left|M_{kj}^{C1}\right|}{\left|S_{k0}\right|\left|S_{j0}\right|\left(T_{S2} - T_{S1}\right)} \tag{3.22}$$

Since the equivalent temperatures of the noise source are measured by the NIR as

$$T_{NS1} = \left|S_{10}\right|^{2}T_{S1} \quad and \quad T_{NS2} = \left|S_{10}\right|^{2}T_{S2} \tag{3.23}$$

the fringe-washing term can be rewritten as

$$G_{kj} = \frac{\left|S_{10}\right|^{2}}{S_{k0}S_{j0}^{*}}\frac{\sqrt{T_{sys_k}^{C2}T_{sys_j}^{C2}}M_{kj}^{C2} - \sqrt{T_{sys_k}^{C1}T_{sys_j}^{C1}}M_{kj}^{C1}}{\left(T_{NS2} - T_{NS1}\right)} \tag{3.24}$$

Note that dependence on the physical temperature of the estimation equation relating G_{kj} has disappeared, even in the general case when physical temperatures are different at the noise distribution network and the LICEF receivers. Moreover, only relative measurements of the S-parameter modulus of the noise distribution network are required. Additionally if we take into account that system temperatures in calibration mode are also measured through the NIR as:

$$\begin{aligned} T_{sys_k}^{C1} &= \frac{v_{1k}-v_{off_k}}{v_{2_k}-v_{1_k}} \frac{|S_{k0}|^2}{|S_{10}|^2} (T_{NS2} - T_{NS1}) \\ T_{sys_k}^{C2} &= \frac{v_{2k}-v_{off_k}}{v_{2_k}-v_{1_k}} \frac{|S_{k0}|^2}{|S_{10}|^2} (T_{NS2} - T_{NS1}) \end{aligned} \tag{3.25}$$

the fringe-wash term can be written as

$$G_{kj} = \frac{\sqrt{(v_{2k} - v_{off_k})(v_{2j} - v_{off_j})} M_{kj}^{C2} - \sqrt{(v_{1k} - v_{off_k})(v_{1j} - v_{off_j})} M_{kj}^{C1}}{\sqrt{(v_{2k} - v_{1k})(v_{2j} - v_{1j})}} \frac{|S_{k0}||S_{j0}|}{S_{k0} S_{j0}^*} \tag{3.26}$$

which only depends on PMS linearity, normalized correlations and the relative phases of the noise distribution network S-parameters.

3.4 Impact of PMS non linearity

As it has been seen in the previous section, the performance of the PMS used to denormalize the digital correlations in interferometric radiometers is degraded due to its non-linear behaviour. In [17] it was shown that the PMS behaviour is very well modelled by means of a second order response:

$$v_k = v_{off_k} + G_k T_{sys_k} + a_k T_{sys_k}^2 \tag{3.27}$$

The non-linear term a_k can not be measured in-orbit by the scheme (four point method) explained in section 3.1 and will introduce an error in the estimation of system temperature. Since non-linearity is assumed to present low sensitivity to temperature, it can be partially corrected from PMS in orbit measurements assuming that an estimation of the non-linear term a_k is availabe from ground measurements. The core of this thesis has been devoted to study different non-linear characterization and correction methods. The following chapters include the results of the work carried out.

Chapter 4

PMS non-linearity measurement test set-up

MIER Comunicaciones [18] was responsible for the design, development and manufacture of the 72 L-band LICEF receivers. These receivers must accomplish very strict requirements: low dispersion, noise figure, high gain and selectvity, low consumption and mass characteristics, and be reliable in space.

MIER COMUNICACIONES developed a methodology to experimentally calibrate and validate the different radiometer prototypes that have been manufactured. Some tests required field experiments, such as measuring the receiver noise figure, including the antenna, which was done by measuring the temperature of sky noise, or measuring and characterizing the non-linearity of PMS. UPC agreed to participate in data processing of EM and PFM tests, providing a tool for real-time monitoring of LICEF EM tests. During the developement of this thesis, the measurement data set provided by MIER has been used to performed the two non-linear characterization measurement methods proposed: the Slope Method and the Deflection Method. For this reason, the following section is devoted to briefly describe the measurement test set-up and the measurement data set.

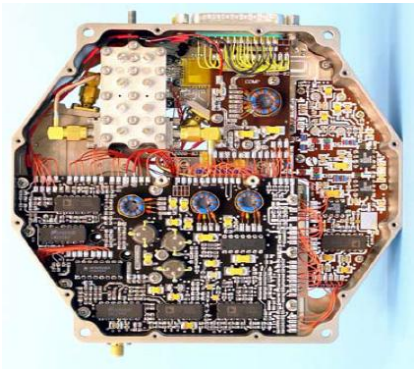

Figure 4.1: EM LICEF-3 flight model manufactured by MIER COMUNICACIONES

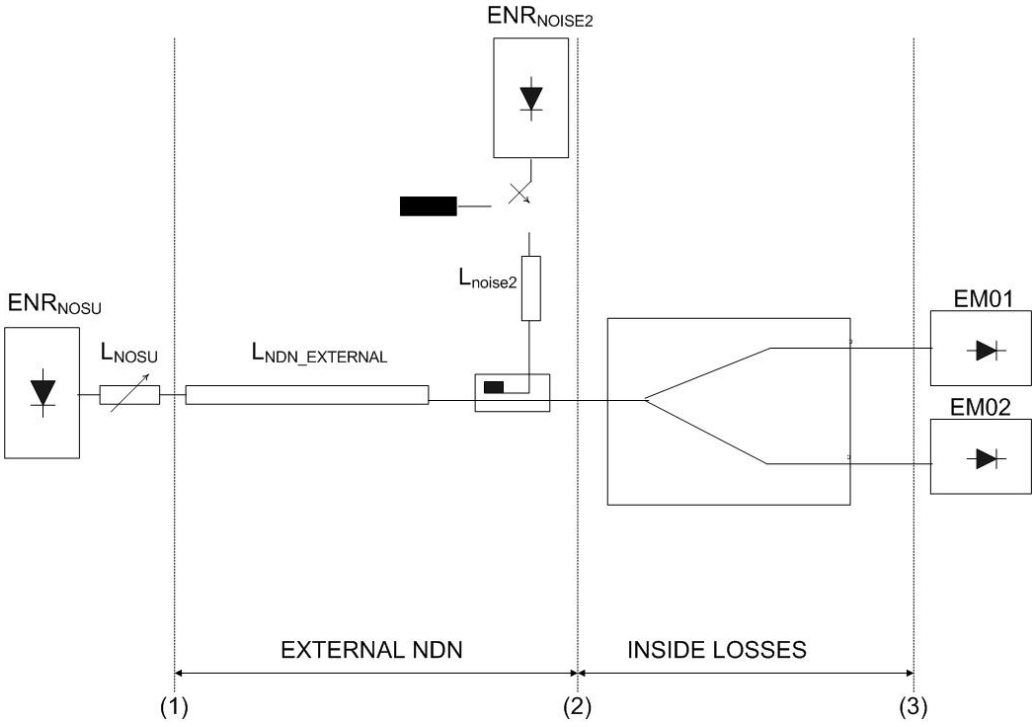

Figure 4.2: PMS linearity test basic setup

4.1 PMS linearity test set-up

The PMS linearity test setup consists in using a directional coupler to add an extra noise to the noise level supplied from NOSU (Noise System Unit). In case the PMS was perfectly linear, this extra noise should produce a constant voltage variation.

The test procedure is the following:

1. Perform the 4-point calibration of the LICEF under test.
2. Set NOise Source the Unit (NOSU) to the minimum power level (maximum attenuation). Acquire 100 samples of output reading voltages
3. Connect the extra Noise Source to the coupler (NS switch position = 2) and acquire 100 samples of the output reading voltages
4. Switch off the extra noise source.
5. Increase the power level of the NOSU. Acquire 100 samples of output reading voltages,
6. Repeat (3) to (7) until the whole power range is covered (11 NOSU levels).

This procedure was performed at three different physical chamber temperatures (5^{o}C, 21^{o}C and 45^{o}C). Hence, the resulting measurement data set consists of 100 samples of

PMS voltages, for each of the 11 levels supplied and for two different configurations: when the extra noise is swithched off and when it is switched on. This is repeatable for each one of the three measurement temperatures (5ºC, 21ºC and 45ºC) and for each receiver.

4.1.1 Summary of equations

This section summarizes the equations and the different steps followed to estimate the system temperature at the input of the LICEF under test, which will be necessary to performe and analyze the two different characterization proposed in this thesis. In order to clarify the procedure, the upper index in all intermidate system temperature is related to the corresponding plane of Figure 4.2.

The procedure of the estimation of the system temperature at the input of the LICEF under test when the extra noise is switched off, and when it is switched on, $T^{(3)}_{in_{OFF}}$, $T^{(3)}_{in_{ON}}$ respectivelly, are detailed in the following subsections (4.1.1.1 and 4.1.1.2).

$L_{EXTERNAL\,NDN} = -12.0809dB$

4.1.1.1 Estimation of System Temperature when extra noise is OFF

The system temperature at the input of LICEF under test (plane (3) in Figure 4.2), when the extra noise is switched off can be estimated following the procedure detailed hereafter:

1. From the Exces Noise Ratio (ENR) of the Noise Source Unit (NOSU), the temperature supplied by the noise source can be computed as:

$$ENR_{NOSU} = 33.75dB \Rightarrow T_{source_{NOSU}} = 290\left[10^{\frac{ENR_{NOSU}}{10}} + 1\right] \tag{4.1}$$

2. Eleven different power levels can be generated, varying the attenuator (L_{NOSU}). Hence, the system temperature at the NOSU output plane (plane (1) in Figure 4.2) can be written as:

$$T^{(1)}_{inOFF} = T_{source_{NOSU}} L_{NOSU} + (T_{phNOSU}\,(1 - L_{NOSU})) \tag{4.2}$$

3. The system temperature up to the TVT (*Thermal Vacumm Test*) chamber (plane (2) in Figure 4.2) can be computed as:

$$T^{(2)}_{inOFF} = T^{(1)}_{inOFF} L_{EXTERNAL\,NDN} + T_{ph}\,(1 - L_{EXTERNAL\,NDN}) \tag{4.3}$$

4. Finally the system temperature at the LICEF under test input (plane (3) in Figure 4.2) when the extra noise is switched off can be estimated as:

$$T^{(3)}_{inOFF} = T^{(2)}_{inOFF} L_{inside} + T_{amb}\,(1 - L_{inside}) \tag{4.4}$$

where $T_{amb}$is the physical chamber temperature and L_{inside} is defined as:

$$L_{inside} = L_{out\,NOSU\,EM01/02} - L_{EXTERNAL\,NDN} \tag{4.5}$$

4.1.1.2 Estimation of System Temperature when extra noise is ON

The system temperature at the input of LICEF under test (plane (3) in Figure 4.2), when the extra noise is switched on can be estimated following the procedure detailed hereafter:

1. The system temperature at the NOSU output plane when the extra noise is switched on is the same that when it is switched off (2):

$$T_{inON}^{(1)} = T_{inOFF}^{(1)} = T_{source_{NOSU}} L_{NOSU} + (T_{phNOSU} (1 - L_{NOSU})) \tag{4.6}$$

2. The system temperature up to the TVT (*Thermal Vacumm Test*) chamber (plane (2) in Figure 4.2) can be computed as:

$$T_{inON}^{(2)} = T_{inON}^{(1)} L_{EXTERNAL\,NDN} + T_{ph} (1 - L_{EXTERNAL\,NDN}) + \\ + T_{N\,source\,2} L_{noise2} \tag{4.7}$$

3. Finally the temperature at the LICEF under test input (plane (3) in Figure 4.2) when the extra noise is switched on can be estimated as:

$$T_{inON}^{(3)} = T_{inON}^{(2)} L_{inside} + T_{amb} (1 - L_{inside}) \tag{4.8}$$

   where $T_{amb}$is the physical chamber temperature and L_{inside} is defined as:

$$L_{inside} = L_{out\,NOSU\,EM01/02} - L_{EXTERNAL\,NDN} \tag{4.9}$$

Chapter 5

The Slope Method

5.1 Introduction

Several methods to characterize the radiometer linearity can be found in the literature [19] [20]. This chapter presents the non-linearity characterization by the so-called Slope Method of the 72 power detectors of each receiver that compouned the MIRAS instrument. This method was used to characterize the non-linearity by Mier Comunicaciones [21], who also performed the set up and the measurements.

During the development of this thesis, this method has been performed using the same measurement data set provided by Mier Comunicaciones. Some slightly differences between both results were found, corrected and reported in [22].

5.2 PMS non linearity characterization

This section presents the PMS non-linearity characterization by the Slope method, which basically consists of the estimation of the second order parameter a_k in expression (3.27). This characterization is based on the measurement set-up described in the previous chapter. As it has been seen, it basically consists off using a directional coupler to add an extra noise to the noise level supplied from NOSU. The rationale of the non linearity characterization is based on a quite simple principle: in case the PMS was perfectly linear, any extra noise should produce a constant voltage variation.

When the extra noise source is turned off the PMS output voltage can be written as a function of input system temprature (plane (3) Figure (4.2)) as:

$$v_{PMS}\left(N_{source} = OFF\right) = v_A = v_{off_k} + G_k^C T_{sys_k}^C + a_k T_{sys_k}^{C2} \tag{5.1}$$

When the extra noise source is turned on, it adds an extra noise $\triangle T_N$ at the LICEF input, and once more considering the second order model of the PMS, the ouptut voltage can be written as a function of input system temperature as:

$$v_{PMS}\left(N_{source} = ON\right) = v_B = v_{off_k} + G_k^C\left(T_{sys_k}^C + \triangle T_N\right) + a_k\left(T_{sys_k}^C + \triangle T_N\right)^2 \tag{5.2}$$

Thus the voltage difference observed at the ouput of PMS can be computed as a function of input system temperature and the extra noise added, substrating expressions (5.1) and (5.2).

$$\begin{gathered}\triangle v_{PMS} = v_{PMS}\left(N_{source} = ON\right) - v_{PMS}\left(N_{source} = OFF\right) = v_B - v_A \\ \triangle v_{PMS} = G_k^C \triangle T_N + a_k\left(\triangle T_N^2 + 2T_{sys_k}^C \triangle T_N\right)\end{gathered} \tag{5.3}$$

Hence, rearranging terms in (5.3) the measured differences in the output voltage will present a linear response with $T_{sys_k}^C$:

$$\triangle v_{PMS} = K_1 + K_2 T_{sys_k}^C \tag{5.4}$$

where,

$$\begin{gathered}K_1 = G_k^C \triangle T_N + a_k \triangle T_N^2 \\ K_2 = 2a_k \triangle T_N\end{gathered} \tag{5.5}$$

So in order to retrieve the second order parameter (a_k), the estimation of the slope (K_2) of delta voltage response ($\triangle v_{PMS}$) with respect to the system temperature (T_{sys}) is needed, as well as, the added extra noise injected ($\triangle T_N$), which has been computed from the measurement data set provided by Mier as:

$$\triangle T_N = T_{in_{ON}}^{(3)} - T_{in_{OFF}}^{(3)} \tag{5.6}$$

where $T_{in_{ON}}^{(3)}$, $T_{in_{OFF}}^{(3)}$ correspond with the system temperature at the LICEF under test input (plane (3) from Figure 4.2), when the extra noise is switched on, and when it is switched off, respectivelly. Their estimation has been detailed in sections 4.1.1.2 and 4.1.1.1, respectively .

Finally, it has been shown that the non linearity term of the PMS can be estimated within the presented mesurement set-up as:

$$a_k = \frac{K_2}{2\triangle T_N} \tag{5.7}$$

5.2.1 Experimental results

This section presents the experimental results of the characterization of second order (a_k) by the Slope Method of all the 72 PMS that compound MIRAS at three different measurement temperatures (5ºC, 21ºC and 45ºC).

In order to clarify the procedure a brief description of the acquired data measured by Mier Comunicaciones is needed. As it has already seen, the basic linearity test setup consists off using a directional couple to add an extra noise to the noise level supplied from NOSU (Figure 4.2). This NOSU supplies 11 different noise levels by varying the attenuator L_{NOSU}. For each PMS unit, for the three different measurement temperatures and for the different 11 noise levels, 100 samples of PMS output readings were measured and stored. This samples were measured for two cases:

- Extra noise source ON
- Extra noise source OFF

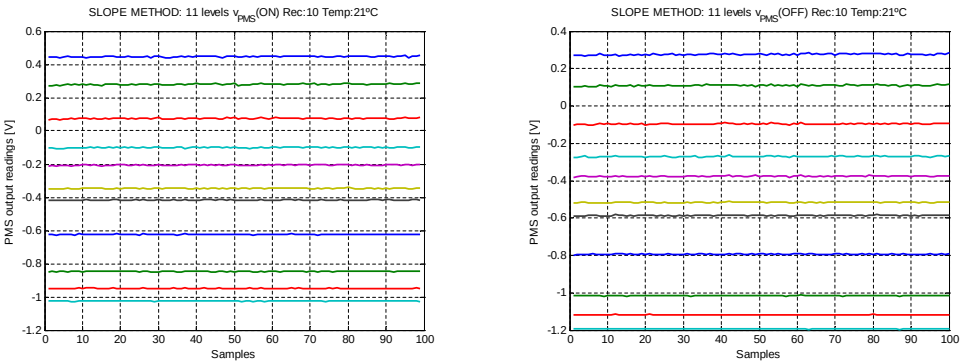

(a) Extra noise source ON

(b) Extra noise source OFF

Figure 5.1: PMS non linearity measurement data set: PMS output readings for the 11 different noise levels supplied by NOSU

Figure 5.1 shows an example of the measurement data set for a particular receiver (number 10) at 21ºC. These 100 PMS output reading samples are avaraged, so its uncertainty is decreased a factor $1/10$, obtaining 11 values for v_A (5.1) and v_B (5.2) respectively. These two magnitudes are used to compute the voltage difference observed (5.3), which is represented as a function of system temperature in Figure 5.2, where the blue points correspond to the measurement data and the green line corresponds to the best first order fit in a least-squares sense. Once the slope of voltage difference (K_2) is estimated in a least-squares sense, the non linearity term a_k can be retrieved from expression (5.7).

Finally Figure 5.3 shows the retrieved values of non linearity term a_k for each one of the measurement temperatures: 5ºC, 21ºC and 45ºC. This non linearity term at 21ºC has been included in the MIRAS Data Base (MDB), and it is usefull to model and analyze the non linearity error (see Chapter 7).

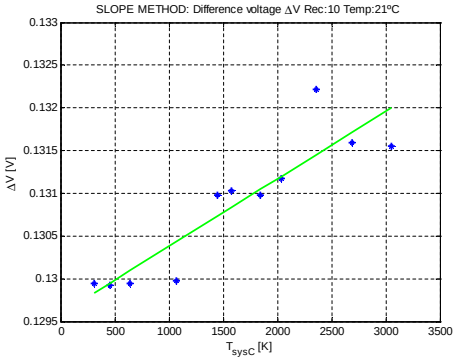

Figure 5.2: Voltage difference Δv as a function of T_{sys}. The blue points correspond to the measurement data and the green line corresponds to the best first order fit in a least-squares sense.

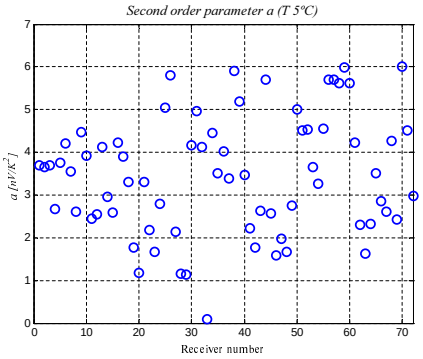

(a) Measurement temperature 5ºC

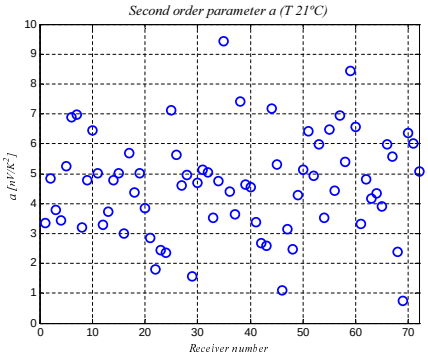

(b) Measurement temperature 21ºC

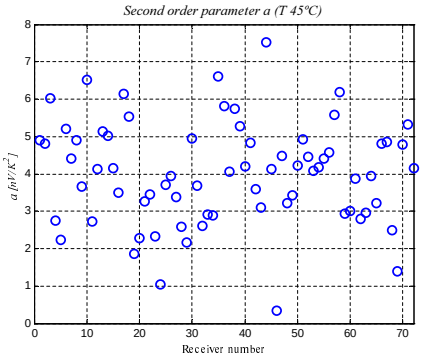

(c) Measurement temperature 45ºC

Figure 5.3: Retrieved second order parameter (a) by the Slope method of the 72 receivers that compound MIRAS at the temperature 5ºC, 21ºC and 45ºC.

5.3 Linearity correction procedure

This section presents the performance of a simple method to correct the second order PMS response even in the case when the diode non-linear behaviour is not perfectly known.

The PMS response is linearized by subtracting from the PMS voltage readings an estimate of the second order contribution. This estimate is computed by assuming a linear behaviour of the PMS. That is, from PMS voltage readings and applying the four-point calibration method can be computed as a first approach as:

$$T_{sys_k}^{SC(1)} = \frac{v_k^{SC(1)} - v_{offk}^{(1)}}{G_{PMS_k}^{(1)}} \tag{5.8}$$

where the superscript (1) indicates that not correction has been done yet.

From the estimated system temperature and from on ground measurements of the PMS second order parameter a_k, the non linearity contribution from the PMS readings can be corrected:

$$v_{ik}^{(2)} = v_{ik}^{(1)} - a_k \left[T_{sys_k}^{SC(1)}\right]^2 \tag{5.9}$$

where the superscript (2) indicates that second order correction has been performed.

Once the non linearity contribution has been corrected, the four point calibration method is again performed in order to obtain a PMS linear model that takes in to account the non linearity correction:

$$\begin{aligned} v_{offk}^{(2)} &= \frac{v_{2k}^{(2)} v_{3k}^{(2)} - v_{1k}^{(2)} v_{4k}^{(2)}}{\left(v_{2k}^{(2)} - v_{4k}^{(2)}\right) - \left(v_{1k}^{(2)} - v_{3k}^{(2)}\right)} \\ G_{PMS_k}^{(2)} &= \frac{v_{2k}^{(2)} - v_{1k}^{(2)}}{|S_{k0}|^2 \sum_{N=1}^{6} \frac{\left(T_{sys_N}^{C_2C} - T_{sys_N}^{C_1C}\right)}{|S_{N0}|^2}} \end{aligned} \tag{5.10}$$

Now the system temperature System temperature at CIPk plane with second order non linear correction can be computed as:

$$T_{sys_k}^{SC(2)} = \frac{v_k^{SC(2)} - v_{offk}^{(2)}}{G_{PMS_k}^{(2)}} \tag{5.11}$$

5.3.1 Summary of equations

Table 5.1 details the step by step equations in order to correct the non-linearity from the PMS output readings by the Slope Method.

5.4 Impact of measurement uncertainty

This section is devoted to asses the impact of errors or uncertainties in the different parameters that are involved in the estimation of the non linear term (a_k).

As it has been shown in section 5.2, the non-linerarity term (a_k) (5.7) can be retrieved from the estimation of the slope (K_2) of the difference voltage observed ($\triangle v$). Figure 5.4 shows a schematic representation of the difference voltage ($\triangle v$) observed as a function of system temperature. The relationship between the different parameters in the figure is detailed hereafter:

$$\left.\begin{array}{c} T_1 \rightarrow v_{A1} \\ T_1 + \triangle T_{N1} \rightarrow v_{B1} \end{array}\right\} \triangle v_1 = v_{B1} - v_{A1}$$
$$\left.\begin{array}{c} T_2 \rightarrow v_{A2} \\ T_2 + \triangle T_{N2} \rightarrow v_{B2} \end{array}\right\} \triangle v_2 = v_{B2} - v_{A2} \tag{5.12}$$

Tanking into account a second order model of the PMS, the difference voltage can be written as:

$$\left.\begin{array}{c} v_{A1} = v_{off} + GT_1 + aT_1^2 \\ v_{B1} = v_{off} + G\left(T_1 + \triangle T_N\right) + a\left(T_1 + \triangle T_N\right)^2 \end{array}\right\} \triangle v_1 = v_{B1} - v_{A1} = G\triangle T_N + a\left(\triangle T_N^2 + 2T_1 \triangle T_N\right)$$

$$\left.\begin{array}{c} v_{A2} = v_{off} + GT_2 + aT_2^2 \\ v_{B2} = v_{off} + G\left(T_2 + \triangle T_N\right) + a\left(T_2 + \triangle T_N\right)^2 \end{array}\right\} \triangle v_2 = v_{B2} - v_{A2} = G\triangle T_N + a\left(\triangle T_N^2 + 2T_2 \triangle T_N\right) \tag{5.13}$$

OUTPUT DATA		
Linearized PMS offset at CIP plane at LICEF calibration temperature (orbit position)	$G_{PMSk}^{C(2)}$ UNITS: [mV/K] $v_{offk}^{(2)}$ UNITS: [V] $T_{sys_k}^{HH(2)}, T_{sys_k}^{HH(2)}, T_{sys_k}^{UV(2)}, T_{sys_k}^{UV(2)}$ UNITS: [K]	
INPUT DATA		
Descript	Variables	Origin
PMS voltages in CAL MODE. 4-point method. The superscript (1) indicates that no correction has been done yet.UNITS [V]	$v_{1k}^{(1)}$,$v_{2k}^{(1)}$,$v_{3k}^{(1)}$,$v_{4k}^{(1)}$	PMS voltages in CAL mode
ANCILLIARY DATA		Origin
Estimation of non linear term [V]	a_k	LICEF PMS characterization by Slope method

STP	EQUATIONS	COMMENT
1	$v_{offk}^{(1)} = \frac{v_{2k}^{(1)} v_{3k}^{(1)} - v_{1k}^{(1)} v_{4k}^{(1)}}{\left(v_{2k}^{(1)} - v_{4k}^{(1)}\right) - \left(v_{1k}^{(1)} - v_{3k}^{(1)}\right)}$ $G_{PMS_k}^{(1)} = \frac{v_{2k}^{(1)} - v_{1k}^{(1)}}{\lvert S_{k0}\rvert^2 \sum_{N=1}^{6} \frac{\left(T_{sys_N}^{C_2C} - T_{sys_N}^{C_1C}\right)}{\lvert S_{N0}\rvert^2}}$	LICEF calibration (4 point method) :PMS gain and offset at CIP plane at LICEF calibration temperature (orbit position)
2	$T_{sys_k}^{SC(1)} = \frac{v_k^{SC(1)} - v_{offk}^{(1)}}{G_{PMS_k}^{(1)}}$	System temperature at CIPk plane. Switch in S=H, V, U positions.
3	$v_{ik}^{(2)} = v_{ik}^{(1)} - a_k \left[T_{sys_k}^{SC(1)}\right]^2$	Linearity correction of PMS readings
4	$v_{offk}^{(2)} = \frac{v_{2k}^{(2)} v_{3k}^{(2)} - v_{1k}^{(2)} v_{4k}^{(2)}}{\left(v_{2k}^{(2)} - v_{4k}^{(2)}\right) - \left(v_{1k}^{(2)} - v_{3k}^{(2)}\right)}$ $G_{PMS_k}^{(2)} = \frac{v_{2k}^{(2)} - v_{1k}^{(2)}}{\lvert S_{k0}\rvert^2 \sum_{N=1}^{6} \frac{\left(T_{sys_N}^{C_2C} - T_{sys_N}^{C_1C}\right)}{\lvert S_{N0}\rvert^2}}$	Calculation of PMS gain and offset from the corrected voltages
5	$T_{sys_k}^{SC(2)} = \frac{v_k^{SC(2)} - v_{offk}^{(2)}}{G_{PMS_k}^{(2)}}$	System temperature at CIPk plane with non linear correction. Switch in S=H, V, U positions.
6	$T_{sys_k}^{HH(2)} = T_{sys_k}^{HC(2)} \frac{\lvert S_{LC_k}\rvert^2}{\lvert S_{LH_k}\rvert^2 \eta_{H_k}}$	System temperature at HAP plane with non linear correction. Switch in H
	$T_{sys_k}^{VV(2)} = T_{sys_k}^{VC(2)} \frac{\lvert S_{LC_k}\rvert^2}{\lvert S_{LV_k}\rvert^2 \eta_{Vk}}$	System temperature at VAP plane with non linear correction. Switch in V
	$T_{sys_k}^{UH(2)} = T_{sys_k}^{UC(2)} \frac{\lvert S_{LC_k}\rvert^2}{\lvert S_{LH_k}\rvert^2 \eta_{H_k}}$	System temperature at HAP plane with non linear correction. Switch in U
	$T_{sys_k}^{UV(2)} = T_{sys_k}^{UC(2)} \frac{\lvert S_{LC_k}\rvert^2}{\lvert S_{LV_k}\rvert^2 \eta_{V_k}}$	System temperature at VAP plane with non linear correction. Switch in U

Table 5.1: Summary of PMS linearity correction by the slope method

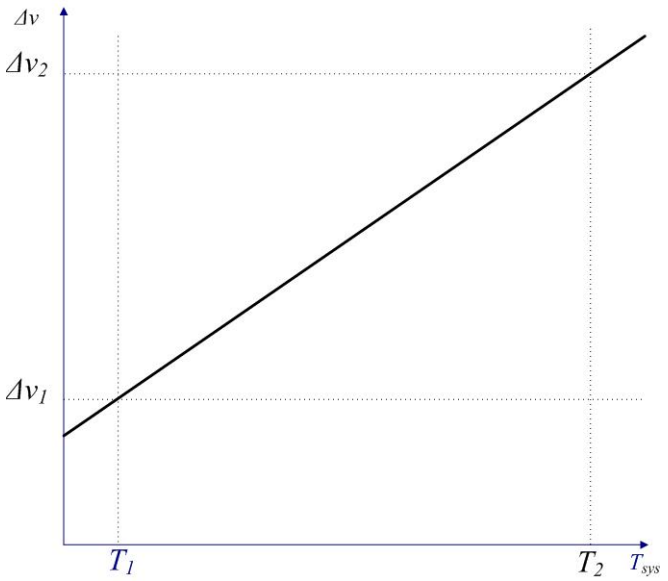

Figure 5.4: Schematic representation of voltage difference Δv as a function of T_{sys}

From Figure 5.4 and from the previous expressions, it is clearly seen that the parameters that most affect the estimation of the non linearity term (a_k) are:

- the extra noise injected ($\triangle T_N$), which absolute value is needed to retrive a_k from the slope (K_2) of the difference voltage ($\triangle v$)
- the uncertainty in PMS output voltages readings, which are also involved in the estimation of the slope K_2
- the uncertainty in input system temperature T_{sys}

The following subsections are devoted to analyze the impact of the uncertainty in these parameters in the measurement of the second order model a by the Slope Method. For this purpose, the Slope Method is simulated, taking into account a second order model of the PMS, which is the mean values of all the receivers, and the same input system temperature that in the experimental case. These values are detailed in table 5.2.

The parameters under study are modeled as a normal random variables of length N, with its mean value and different values of standard deviation. Hence for each standard deviation value considered, and after performing the Slope method, N values of the second order parameter a are obtained, representing N different realizations of the experiment. Thus the uncertainty of the second order parameter σ_a can be evaluated as a function of the uncertainty of the parameter under study.

Another way to evaluate the impact of the uncertainty of these parameters in the measurement of the second order parameter a, is computing the relative error of the mean of all realizations $\langle \hat{a} \rangle$ with respect to the nominal case a considered in the simulations. This error can be computed as:

$T_A\,[K]$	0,100,200,300,500,700,900,1100,1300,1500
$T_O\,[K]$	290
$T_r\,[K]$	180
$\Delta T_N\,[K]$	136
T_{AN}	$T_A + \Delta T$
T_{ON}	$T_O + \Delta T$
T_{sysX}	$T_X + T_r$ $where\, X = A, O, AN, ON$
PMS second order Model	$a = 4.4875\,\mathrm{nV/K^2}$ $G = 1.2\,\mathrm{mV/K}$ $v_{off} = -1.7818\,V$
N:Number of measurement realizations	1000

Table 5.2: Parameters of the simulation of the impact of measurement uncertainty by Slope Method

$$error_X\,[\%] = \frac{\langle \hat{a} \rangle - a}{a} \cdot 100 \tag{5.14}$$

where X stands for the parameter under study: $\triangle T_N$, v_{PMS} or T_{sys}.

5.4.1 Impact of uncertainty in $\triangle T_N$

In this section the impact of uncertainty in the extra noise injected $\triangle T_N$ in the measurement of the second order parameter (a) is evaluated. For this purpose, the slope method has been simulated, considering that the extra noise injected $\triangle T_N$ involved in the procedure is modeled as random variable with its mean and different standard deviation values.

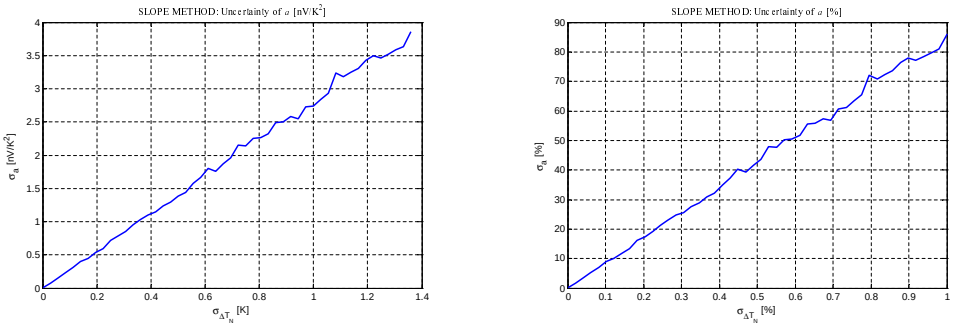

(a) Absolute [nV/K] (b) Relative [%]

Figure 5.5: Uncertainty of a as a funciton of untertainty in $\triangle T_N$

Figure 5.5 shows the uncertainty of the second order parameter as a function of the uncertainty in the extra noise injected $\triangle T_N$.

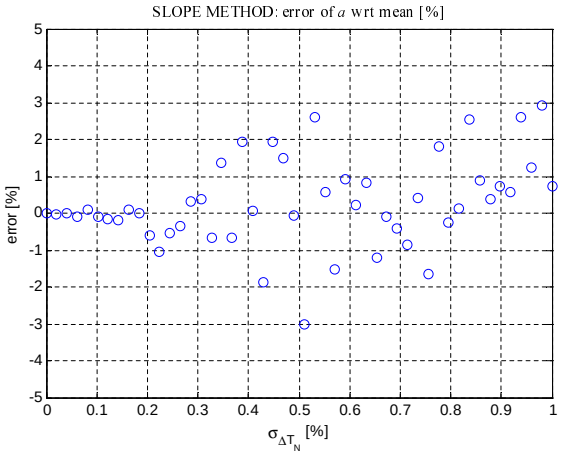

Figure 5.6: Error of a [%] wrt the mean as function of uncertainty in $\triangle T_N$ [%]

Figure 5.6 shows the error of the parameter a with respect to the mean as a function of uncertainty in the extra noise injected $\triangle T_N$. However, $\triangle T_N$ is more likely to present a systematic error (bias) than a random error and these results are not very significative. The impact of a systematic error in $\triangle T_N$ is analyzed in section 5.4.4.

5.4.2 Impact of uncertainty in PMS output voltage readings

In this section the impact of uncertainty in PMS output voltage readings in the measurement of the second order parameter (a) is evaluated. For this purpose, the slope method has been simulated, considering that all the PMS output voltages involved in the procedure are modeled as random variables with their mean and different standard deviation values.

Figure 5.7 shows the uncertainty in the second order model as a function of the uncertainty in the PMS output voltages.

Figure 5.8 shows the error of the parameter a with respect to the mean as a function of uncertainty in the ouput voltage readings.

As it can be seen in the figure 5.7 the slope method is very sensitive to the uncertainty in the PMS voltage, for an uncertainty of 0.1% we obtain an uncertainty in the second order parameter (a) over 100%. Regarding the mean, the error for the same uncertainty value in the PMS voltage is over 1% (Figure 5.8).

5.4.3 Impact of uncertainty in System Temperature

In this section the impact of uncertainty in system temperature in the measurement of the second order parameter (a) is evaluated. For this purpose, the slope method has been simulated, considering that all the system temperatures involved in the procedure are modeled as random variables with their mean and different standard deviation values.

Figure 5.9 shows the uncertainty in the second order model as a function of the uncertainty in the PMS output voltages.

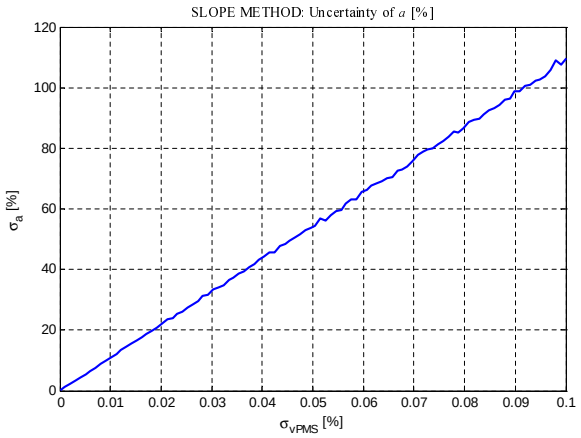

Figure 5.7: Uncertainty of a [%] as a function of uncertainty in output voltage readings [%]

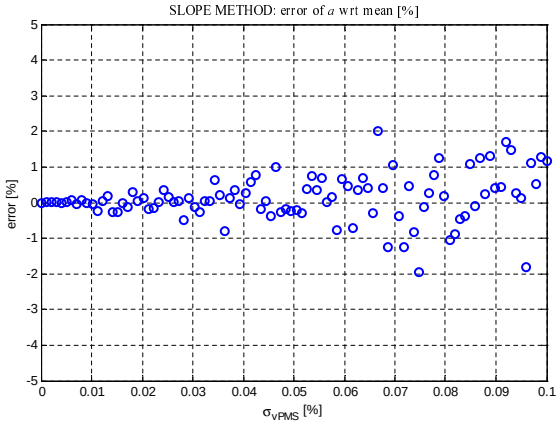

Figure 5.8: Error of a [%] wrt the mean as a function of uncertainty in output voltage readings [%]

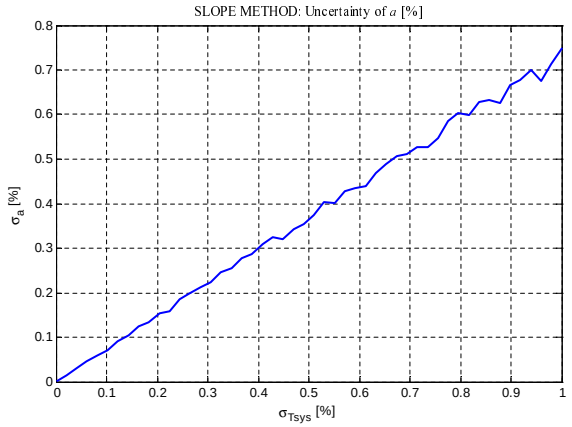

Figure 5.9: Uncertainty of a [%] as function of uncertainty in system temperature [%]

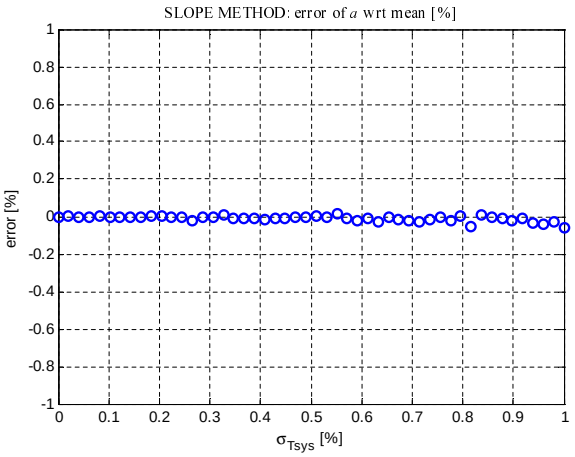

Figure 5.10: Error of a [%] wrt the mean as function of uncertainty in system temperature [%]

Figure 5.10 shows the error of the parameter a with respect to the mean as a function of uncertainty in the system temperature.

As it can be in figures 5.9 and 5.10 the uncertainty in the system temperature has practically no effect in the measurement of the second order parameter, when comparing with the uncertainty in the PMS output voltage readings.

5.4.4 Impact of systematic error in $\triangle T_N$

In order to evaluate the impact of systematic error in the measurement of a parameter, different simulated measurements have been performed considering different values of the extra noise injected $\triangle T_N$ [126 K, 146 K], and then, when the a parameter is retrieved

(5.7), the mean value of $\triangle T_N$ (136 K) is considered.

The left plot of Figure 5.11 shows the retrieved a parameter versus the different values of $\triangle T_N$ considered (in red) and the value of the parameter $a\,(4.4875\,^{nV}/_{K^2})$ considered in order to make simulations in green. The right plot represents the error of the retrieved a with respect to the mean value versus the systematic error of $\triangle T_N$.

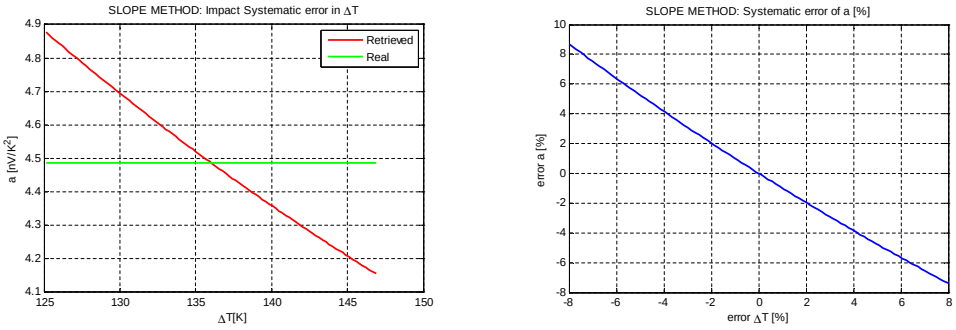

(a) Absolute units

(b) Relative [%]

Figure 5.11: Impact of a systematic error in $\triangle T_N$ in the measurement of a

As it can be seen, an error in $\triangle T_N$ translates directly in the estimation of a.

5.5 Conclusions

This section is devoted to summarize the main conclusion of this chapter.

A method to characterize the non-linearity of the PMS has been presented. It basically consists of estimating the second order parameter a_k, which models the non-linearity of power detector as a function of the system temperature at plane C. This second order response is a useful tool to model the non-linearity of the detector and allows to perform different studies such as the impact of measurement uncertainties, which has been presented in this chapter.

Regarding the impact of measurement uncertainty, it has been seen that the main sources of error in the measurement of a by the Slope method depends on:

- systematic errors in the extra noise injected (ΔT_N), which translate directly in the estimation of a,
- the uncertainty in the PMS output readings,
- the uncertainty in the knowledge of input system temperature T_{sys} (Figure 5.2).

Chapter 6

Deflection Method

6.1 Introduction

The constant deflection method [23] has been used to test and characterize the radiometer linearity. Using this approach, non-linearities are observed as deviations of the noise diode deflection as the antenna noise temperature changes. This method offers the advantage that it can be applied to the complete radiometer system.

The PMS linearity test set up was described in section 4.1, it basically consists of using a directional coupler to add an extra noise to the noise level supplied from NOSU. This extra noise ($\triangle T_N$) may be sufficient to characterize the linearity of the PMS, since if it was perfectly linear, this added extra noise should produce a constant voltage variation. Hence the linearity can be examined with the following ratio:

$$D = \frac{v_{AN} - v_A}{v_{ON} - v_O} \tag{6.1}$$

Where the four voltages represent the response to the NOSU power supplied (v_A), NOSU plus extra noise diode (v_{AN}), temperature reference (v_O) and reference plus extra noise diode (v_{ON}) respectivelly .

If the PMS second order model is considered, any detected voltage can be written as a function of input system temperature, by the following well-kown expression:

$$v_{det} = v_{off} + GT_{sys} + aT_{sys}^2 \tag{6.2}$$

Then the deflection ratio can be written as:

$$\left.\begin{array}{l} v_{AN} - v_A = a\left(\triangle T_N^2 + 2T_A\triangle T_N\right) + G\triangle T_N \\ v_{ON} - v_O = a\left(\triangle T_N^2 + 2T_O\triangle T_N\right) + G\triangle T_N \end{array}\right\} D = \frac{a\left(\triangle T_N^2 + 2T_A\triangle T_N\right) + G\triangle T_N}{a\left(\triangle T_N^2 + 2T_O\triangle T_N\right) + G\triangle T_N} \tag{6.3}$$

Hence in the case that the PMS has a perfectly linear behavior ($a = 0$), the deflection ratio D is equal to 1. Therefore the Deflection ratio is a good and simple technique to measure non-linearities in the end to end radiometer system.

On the other hand, it is possible to perform a new non linearity correction at a voltage level.

If a first estimation of v_{off}, by the 4 point method or by a first order fit, is considered, then it is posible to work with a zero mean signal $v_{det}^{'}$ as:

$$v_{det}^{'} = v_{det} - v_{off} = GT_{sys} + aT_{sys}^2 \tag{6.4}$$

Now if it is taken into account that the linearized voltage can be written as:

$$v_{lin} = GT_{sys} \tag{6.5}$$

then expression (6.4) can be written as a funcion of the linearized voltage as:

$$v_{det}^{'} = v_{det} - v_{off} = GT_{sys} + aT_{sys}^2 = v_{lin} + \frac{a}{G^2} v_{lin}^2 \tag{6.6}$$

Hence if the following second order equation is solved, the linearized voltage v_{lin} can be written as a function of the low signal detected voltage $v_{det}^{'}$:

$$\begin{array}{c} \frac{a}{G^2} v_{lin}^2 + v_{lin} - v_{det}^{'} = 0 \\ v_{lin} = -\frac{G^2}{2a} \pm \sqrt{\frac{G^4}{4a^2} + \frac{G^2}{a} v_{det}^{'}} \end{array} \tag{6.7}$$

If a correction factor C is defined as:

$$C = \frac{G^2}{2a} \tag{6.8}$$

expression (6.7) can be rewritten as:

$$v_{lin} = C\sqrt{1 + \frac{2}{C} v_{det}^{'}} - C \tag{6.9}$$

Thus, once the correction parameter C is estimated or measured, it can be used to correct the non-linear contribution of any detected voltages. Section 6.2 details the procedure proposed in order to measure and retrieve the correction parameter C, while section 6.3 details the non-linearity correction in the current calibration scheme of MIRAS.

6.2 Characterization of non linearity

In order to estimate the value of C the following procedure has been applied. The mean steps are summarized hereafter:

1. Compute the deflection coefficient D as a function of T_{sys}. This step is used exclusively to display the non-linearity effect, but not to process the data.

$$D = \frac{v_{AN} - v_A}{v_{ON} - v_O} \tag{6.10}$$

2. Compute v_{off} by the four point method and remove it from the voltages measurement set.

$$\begin{array}{c} v_{off} = \frac{v_2 v_3 - v_1 v_4}{(v_2 - v_4) - (v_1 - v_3)} \\ v_A^{'} = v_A - v_{off} \\ v_{AN}^{'} = v_{AN} - v_{off} \\ v_O^{'} = v_O - v_{off} \\ v_{ON}^{'} = v_{ON} - v_{off} \end{array} \tag{6.11}$$

3. Perform a swept of posible candidates values of C, linearized the voltages data set and compute a linearized Deflection ratio.

$$\left.\begin{aligned} v_{A\,lin} &= C\sqrt{1+\tfrac{2}{C}v'_A} - C \\ v_{AN\,lin} &= C\sqrt{1+\tfrac{2}{C}v'_{AN}} - C \\ v_{O\,lin} &= C\sqrt{1+\tfrac{2}{C}v'_O} - C \\ v_{ON\,lin} &= C\sqrt{1+\tfrac{2}{C}v'_{ON}} - C \end{aligned}\right\} D_{lin} = \frac{v_{AN\,lin} - v_{A\,lin}}{v_{ON\,lin} - v_{O\,lin}} \tag{6.12}$$

4. Define the error function as:

$$error\,[\%] = \sqrt{\frac{1}{N-1}\sum_{i=1}^{N-1}\left(D_{lin_i} - 1\right)^2} \cdot 100 \tag{6.13}$$

Where N is the number of noise level supplied by the noise source. Note that the upper index in the sum is N-1, since the lower level of the Noise Source is used as a reference voltage (v_{ON} , v_O) in the computation of Deflection ratio and the other 10 levels are used to compute the numerator of the Deflection ratio D in expression (6.12).

5. Find minimum error by sweeping C, that is, for each value of the sweep, compute the error function defined in step 3. The estimated value of C is the one that minimizes the error function.

The main advantage of this method consists of not requiring the absolute calibration of the injected noise ΔT_N, as well as, the knowledge of T_{sys}. The value of C is obtained directly.

6.2.1 Experimental results

This method has been applied in order to characterize the non-linearity by Deflection Method, using the same data set available from the linearity test (slope method) performed and measured by Mier. That is, the estimation of the correction parameter C, for all the 72 receivers that compouned MIRAS instrument, and for each of the three measurement temperatures (5ºC, 21ºC and 45ºC) has been performed. A large effort of this thesis has been devoted to characterized and measure the non linearity by the Deflection Method. All this work has been reflected in different Technical Notes, however for the sake of simplicity, in this thesis only the intermidiate steps and the final results are included, in order to give an overview of the proposed method.

To sum-up, the characterization of non linearity by the Deflection Method basically consists of performing a swept of posible values of C, linearizing all the PMS voltages, recomputing a linearized Deflection Ratio (D_{lin}) and its rms error with respect to the theoretical value ($D_{lin} = 1$) . The retrieved value of C is the one that minimizes this rms error.

Figure 6.1 shows an example of the error function to minimize as a fuction of the swept values of C. As it can be seen, this function presents a clear minimum, that corresponds to the retrieved value of C. In order to check the correct performance of the method, once the value C is retrieved, the Deflection ratio is represented (Figure 6.2) for both cases: before (red plot) and after (green plot) applying the linearization correction. As it is shown in Figure 6.2, the Deflection ratio once the correction is performed is about

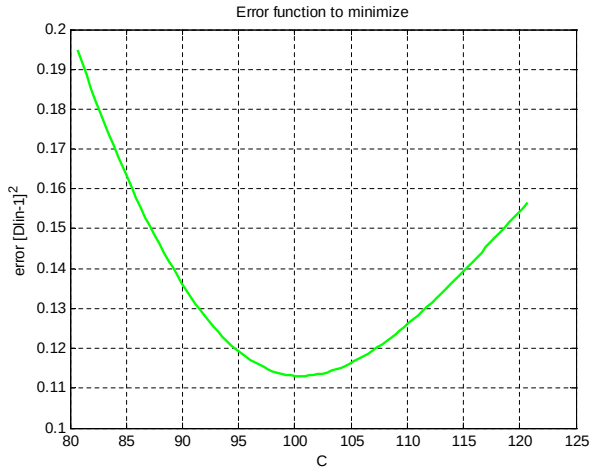

Figure 6.1: Error function to minimize as a function of C

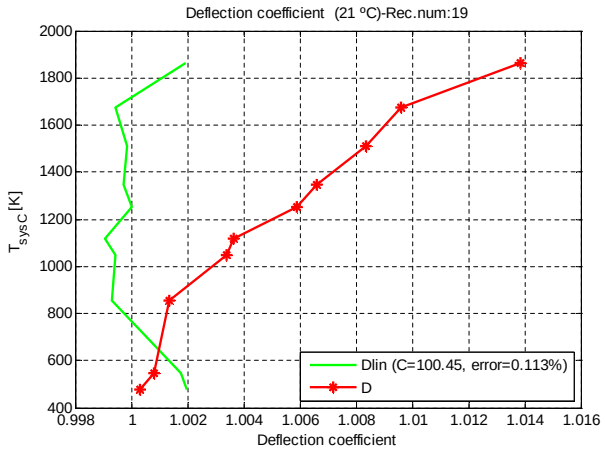

Figure 6.2: Deflection ratio, green line corresponds to the linearized defection ratio and the red one to the deflection ratio without any correction.

1, what indicates that the correction has been applied properly. The legend of the figure also indicates the retrieved value of C used to linearize the voltages, as well as the rms error obtained.

Finally Figure 6.3 shows the retrieved values of C for each one of the measurement temperatures: 5ºC, 21ºC and 45ºC. This retrieved correction parameter at 21ºC have been included in the MDB (Miras Data Base) and they will be used in the official SMOS Level-1 processor, as well as in the MIRAS-TS developed by UPC, in order to correct the non-linearity of the detectors.

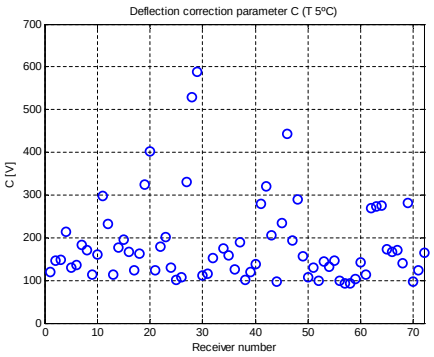

(a) Measurement temperature 5ºC

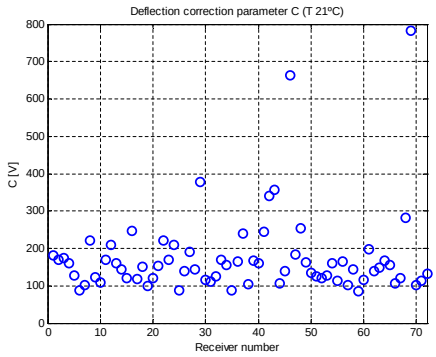

(b) Measurement temperature 21ºC

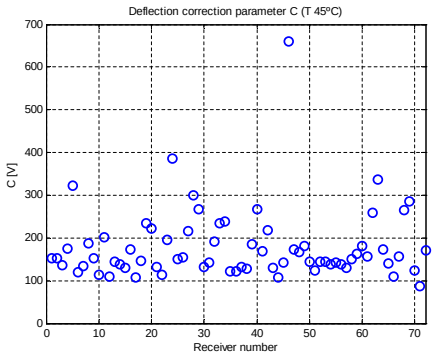

(c) Measurement temperature 45ºC

Figure 6.3: Retrieved non linearity correction parameter (C) by Deflection Method of the 72 receivers that compound MIRAS at different physical temperature 5ºC, 21ºC and 45ºC.

6.2.2 Deflection Testing Software

Deflection Testing Software, from now on DTS, is a tool designed during the developement of this thesis. The main objective of this software package is to measure and characterize the non linearity by the Deflection Method, although it also has another package to asses the stability of the detector by means of the Allan Variance.

The Software is capable to read and process automatically the measurement data set files, in order to characterize the non linearity of the PMS, following the procedure explained in this section.

Figure 6.4 shows the user graphical interface of DTS. As it can be seen in the figure, the software shows the same intermidate graphics that have been presented in last section in order to check the correct performance of the measurement. The other two graphics correspond to the non-linear error and the residual non-linear error, respectivelly, as a function of system temperature. These two error definitions are presented in Chapter 7. It is worth to mention, that the software also performes the characterization of non-linearity by the slope method, which is necessary to compute these errors.

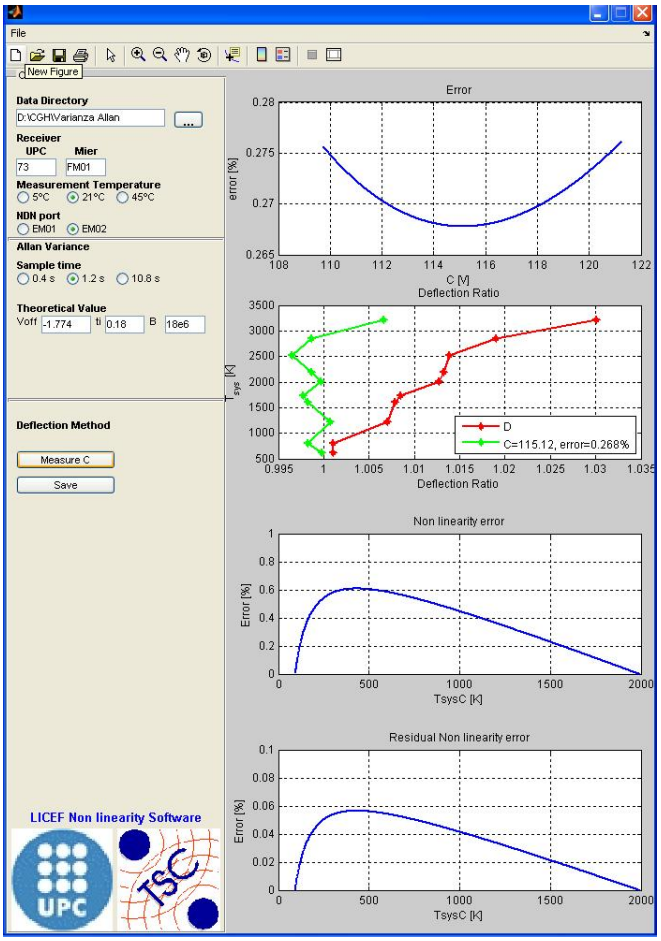

Figure 6.4: User graphical interface of Deflection Testing Software

6.3 Linearity correction procedure

This section presents the performance of the Deflection method to correct the second order contribution of the PMS response.

Linearity correction procedure by Deflection method is an iterative procedure in which PMS response is linearized from PMS voltage readings or detected voltages (v_{det}) directly as:

$$v_{lin} = C\sqrt{1 + \frac{2}{C}v_{det}} - C \tag{6.14}$$

As it has been already said, the parameter C has been estimated using same data set available from linearity test performed and measured by Mier following the procedure explained in section 6.2. Therefore it allows to correct non linearity response of PMS from on ground characterization of each PMS. This linearization expression (6.14) can

only be applied to a zero offset voltage, hence the offset voltage has to be first estimated in order to subtract it from the PMS voltage readings, and that makes the linearization procedure an iterative method. So first, considering a lineal model of PMS, the offset voltage is estimated by the four point method:

$$v_{offk}^{(1)} = \frac{v_{2k}^{(1)} v_{3k}^{(1)} - v_{1k}^{(1)} v_{4k}^{(1)}}{\left(v_{2k}^{(1)} - v_{4k}^{(1)}\right) - \left(v_{1k}^{(1)} - v_{3k}^{(1)}\right)} \tag{6.15}$$

Once the first estimation of the offset voltage is obtained, it is subtracted to the four voltages involved in the four point method, in order to linearize them with expression (6.14):

$$\begin{aligned} v_{ik}^{'} &= v_{ik}^{(1)} - v_{offk}^{(1)} \\ v_{ik}^{(2)} &= C_k \sqrt{1 + \tfrac{2}{C_k} v_i^{'}} - C_k \end{aligned} \tag{6.16}$$

where superscript (1) indicates that no correction has been performed yet, and (2) indicates that the voltage has been corrected or linearized, whereas the subscript i stands for the four point voltages (from 1 to 4) and the subscript k stands for the receiver name (from 1 to 72) .

The following step in order to compute a linearized offset voltage is compute the residual offset by the four point method, taking in to account the linearized voltages.

$$v_{offk}^{res} = \frac{v_{2k}^{(2)} v_{3k}^{(2)} - v_{1k}^{(2)} v_{4k}^{(2)}}{\left(v_{2k}^{(2)} - v_{4k}^{(2)}\right) - \left(v_{1k}^{(2)} - v_{3k}^{(2)}\right)} \tag{6.17}$$

Hence the linearized offset will be the contribution of (6.15) and (6.17):

$$v_{offk}^{(2)} = v_{offk}^{(1)} + v_{offk}^{res} \tag{6.18}$$

Once the linearized offset $v_{offk}^{(2)}$has been computed, any PMS voltage can be linearized by:

$$\begin{aligned} v_{k}^{'} &= v_{k}^{(1)} - v_{offk}^{(2)} \\ v_{k}^{(2)} &= C_k \sqrt{1 + \tfrac{2}{C_k} v_k^{'}} - C_k \end{aligned} \tag{6.19}$$

where $v_k^{(1)}$is the PMS voltage reading to linearize and $v_k^{(2)}$is the linearized one and the subscript k incidicates the receiver number.

6.3.1 Summary of equations

Table 6.1 shows the step by step equations in order to linearized the calibration voltages and computed a offset voltage that takes into account the linearization by Deflection Method. Note that if no correction is performed, the output data will be: $v_{offk}^{(2)} = v_{offk}^{(1)}$

Whereas, Table 6.2 shows the step by step equations in order to linearized any other voltages by Deflection Method. Note that if no correction is performed, the output data will be: $v_k^{(2)} = v_k^{(1)} - v_{offk}^{(2)}$, where $v_{offk}^{(2)}$ was not linearized in the calibration procedure.

OUTPUT DATA		
Linearized PMS offset at CIP plane at LICEF calibration temperature (orbit position)	$v_{offk}^{(2)}$ UNITS: [V]	
INPUT DATA		
Descript	Variables	Origin
PMS voltages in CAL MODE. 4-point method. The superscript (1) indicates that no correction has been done yet.UNITS [V]	$v_{1k}^{(1)}$,$v_{2k}^{(1)}$,$v_{3k}^{(1)}$,$v_{4k}^{(1)}$	PMS voltages in CAL mode
ANCILLIARY DATA		Origin
Estimation of non linear term [V]	C_k	LICEF PMS characterization by Deflection method

STP	EQUATIONS	COMMENT
1	$v_{offk}^{(1)} = \frac{v_{2k}^{(1)} v_{3k}^{(1)} - v_{1k}^{(1)} v_{4k}^{(1)}}{\left(v_{2k}^{(1)} - v_{4k}^{(1)}\right) - \left(v_{1k}^{(1)} - v_{3k}^{(1)}\right)}$	Computation of a first estimation of PMS offset
2	$v_{ik}^{'} = v_{ik}^{(1)} - v_{offk}^{(2)}$ $v_{ik}^{(2)} = C_k \sqrt{1 + \frac{2}{C_k} v_{ik}^{'}} - C_k$	Linearity correction of PMS readings.Before correction offset has to be removed from PMS readings.
3	$v_{offk}^{res} = \frac{v_{2k}^{(2)} v_{3k}^{(2)} - v_{1k}^{(2)} v_{4k}^{(2)}}{\left(v_{2k}^{(2)} - v_{4k}^{(2)}\right) - \left(v_{1k}^{(2)} - v_{3k}^{(2)}\right)}$ $v_{offk}^{(2)} = v_{offk}^{(1)} + v_{offk}^{res}$	Computation of linearized PMS offset from corrected voltages.

Table 6.1: Summary of PMS linearity correction of calibration voltages

6.4 Impact of measurement uncertainty

6.4.1 Impact of uncertainty in PMS output voltage readings

In this section the impact of uncertainty in PMS output voltage readings in the measurement of the parameter C is evaluated. For this purpose, the deflection method has been simulated, considering all the PMS output voltages involved in the procedure are modeled as random variable with their mean values and standard deviation . In order to evaluate this impact, the Deflection method procedure explained before has been simulated considering the second order model of a typical PMS (a=4.4875 [$^{nV}/_{K^2}$], G= 1.2 [$^{mV}/_{K}$], v_{off}= -1.7818 [V]). Table 6.3 summarizes other parameters of the simulation, such as: the ten levels of input system temperature, references level, and equivalent noise temperature.

Figure 6.5 shows the uncertainty in the measurement of C parameter, by the procedure explained in previous sections, as a function of the uncertainty in PMS output voltage readings.

Figure 6.6 shows the intermediate steps of the evaluation of the impact of PMS output

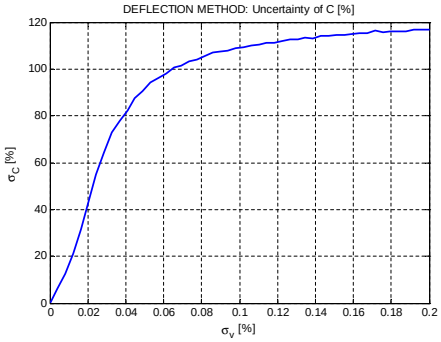

Figure 6.5: Error of C [%] wrt the mean as a function of uncertainty in output voltage readings [%]

readings in the measurement of C parameter by the deflection method for different values of uncertainty in PMS voltages output readings. The graphics from the left column show the error function to be minimized by sweeping C, presented and defined in section 6.2, and the graphics from the right column represent the retrieved C in order to show its distribution or standard deviation.

The graphics show that for lower values of uncertainty in PMS output voltages readings, the function error to minimize has a clearly defined minimum, and so the retrieved value of the C parameter is the same for each realization. As the uncertainty of PMS voltage is increased, the minimum of the error function is wider and the standard deviation of the retrieved C also increases (clouds of points of retrieved C are wider). For uncer-

OUTPUT DATA		
Zero offset linearized PMS voltages UNITS [V]	$v_k^{(2)}$ UNITS: [V]	
INPUT DATA		
Description	Variables	Origin
Linearized PMS offset voltage. UNITS [V]	$v_{offk}^{(2)}$,$v_k^{(1)}$	PMS offset at CIP plane at LICEF calibration temperature and PMS voltage reading to be linearized.
ANCILLIARY DATA		Origin
Estimation of non linear term [V]	C_k	LICEF PMS characterization by Deflection method

STP	EQUATIONS	COMMENT
1	$v_k^{'} = v_k^{(1)} - v_{offk}^{(2)}$ $v_k^{(2)} = C_k\sqrt{1+\frac{2}{C_k}v_k^{'}} - C_k$	Computation of a first estimation of PMS offset

Table 6.2: Summary of PMS linearity correction of other voltages

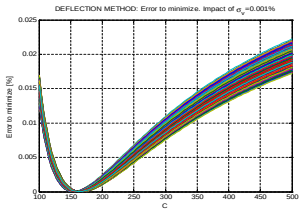

(a) Error to minimize $\sigma_v = 0.001\%$

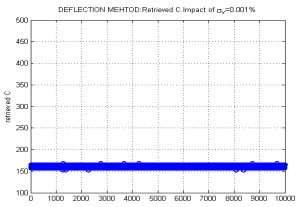

(b) Retrieved C parameter $\sigma_v = 0.001\%$

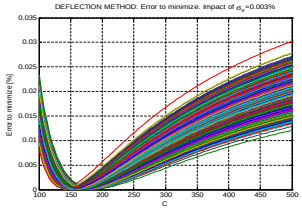

(c) Error to minimize $\sigma_v = 0.003\%$

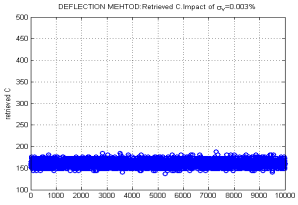

(d) Retrieved C parameter $\sigma_v = 0.003\%$

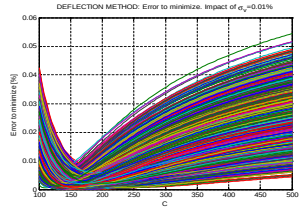

(e) Error to minimize $\sigma_v = 0.01\%$

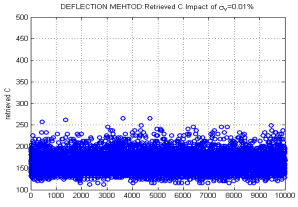

(f) Retrieved C parameter $\sigma_v = 0.01\%$

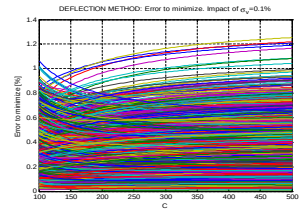

(g) Error to minimize $\sigma_v = 0.1\%$

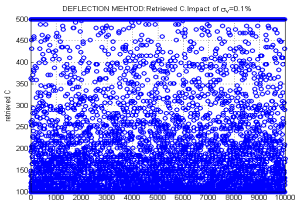

(h) Retrieved C parameter $\sigma_v = 0.1\%$

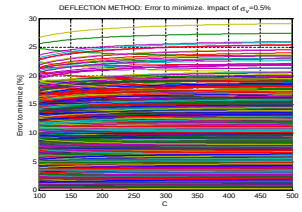

(i) Error to minimize $\sigma_v = 0.5\%$

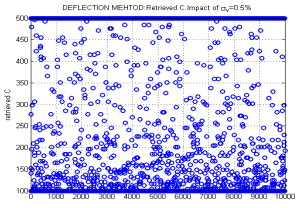

(j) Retrieved C parameter $\sigma_v = 0.5\%$

Figure 6.6: Impact of uncertainty in PMS voltage readings

$T_A\,[K]$	0,100,200,300,500,700,900,1100,1300,1500
$T_O\,[K]$	290
$T_r\,[K]$	180
$\Delta T_N\,[K]$	136
T_{AN}	$T_A + \Delta T$
T_{ON}	$T_O + \Delta T$
T_{sysX}	$T_X + T_r$ $where\, X = A, O, AN, ON$

Table 6.3: Parameters of the simulation of the impact of uncertainty in PMS output

tainties of PMS output voltages readings values higher than 0.01%, the error function does not present a defined minimum, and the retrieved value of C parameter correspond to extremes of the interval of the sweep, since as it has been in section 6.2 the C retrieved value is the one that minimizes the error function.

It could be concluded that when the uncertainty in the PMS output readings is comparable to the function error to be minimized, the value of C parameter can not be correctly retrieved. That is, in order to characterize non-linearity by the Deflection Method, these non-linearity error should be higher than the noise, e.g.: if non-linearity error is about 0.2 %, in order to properly characterize this non-linearity, the noise level should be below 0.02%.

6.4.2 Impact of reference level

This section evaluates the impact of the reference level (T_O, v_O) selected in order to compute the Deflection Coefficient (6.1) in the estimation of C parameter by the deflection method. For this purpose, same procedure than the one followed in the last section has been applied, but for different values of T_O.

In this case, the uncertainty in PMS voltages output readings selected is 0.02% for all cases. The reason of selecting this uncertainty is due to the PMS uncertainty is about 0.18%, and since there are 100 measurements of each level this uncertainty is reduced a factor of $\sqrt{100}$ (0.018%) by averaging. In a similar way than in the last section, the graphics from the left column show the error function to be minimized by sweeping C, presented and defined in section (6.2), and the graphics from the right column represent the retrieved C in order to show its distribution or standard deviation, for different values of T_O.

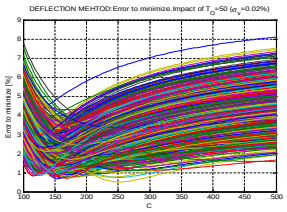

(a) Error to minimize $T_O = 50\,K$

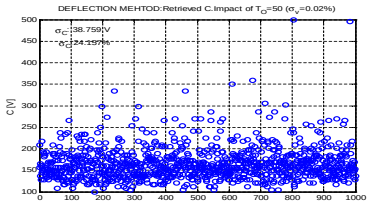

(b) Retrieved C parameter $T_O = 50\,K$

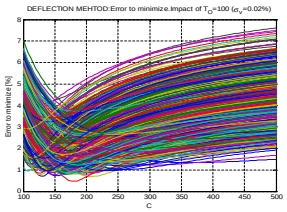

(c) Error to minimize $T_O = 100\,K$

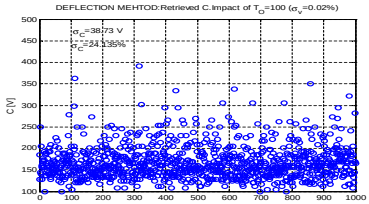

(d) Retrieved C parameter $T_O = 100\,K$

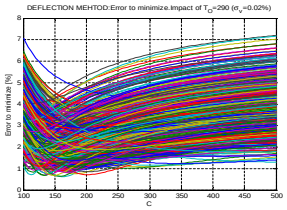

(e) Error to minimize $T_O = 290\,K$

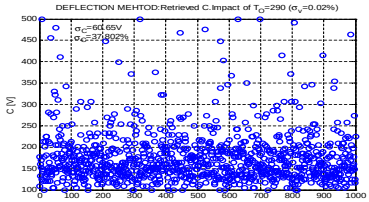

(f) Retrieved C parameter $T_O = 290\,K$

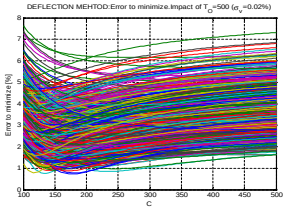

(g) Error to minimize $T_O = 500\,K$

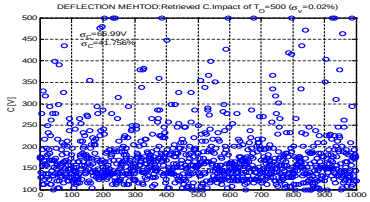

(h) Retrieved C parameter $T_O = 500\,K$

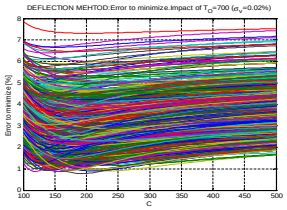

(i) Error to minimize $T_O = 700\,K$

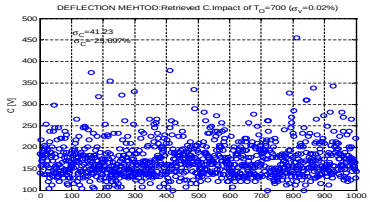

(j) Retrieved C parameter $T_O = 700\,K$

Figure 6.7: Impact of reference level in the characterization of non-linearity by the Deflection method ($\sigma_v = 0.02\%$).

As it is shown in Figure 6.7 the uncertainty in C increases for higher values of reference levels of T_O. Since the reference level has a high impact in the estimation of C by the Deflection method, in order to reduce the impact in the uncertainty of C, v_O has to be well determined or known, that means that its uncertainty has to be low or in the present measurement set-up schema, it would be necessary to take more samples of the reference voltage v_O . Figure 6.8 shows the impact of reducing the uncertainty of reference level a factor 10 respect to the uncertainty of the other PMS output reading involved in the procedure ($\sigma_{v_{A,AN}} = 0.02\%$, $\sigma_{v_{O,ON}} = 0.002\%$). Within the present measurement test set-up, it means measuring 100 samples for v_{AN} and v_A, and 10.000 samples for v_{ON} and v_O.

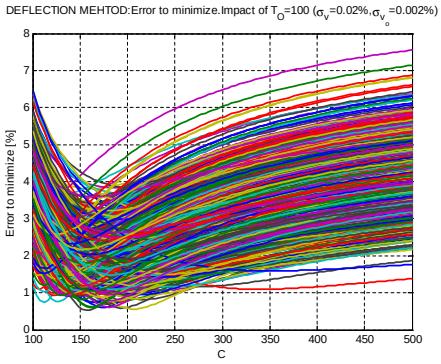

(a) Error to minimize $T_O = 100\,K$

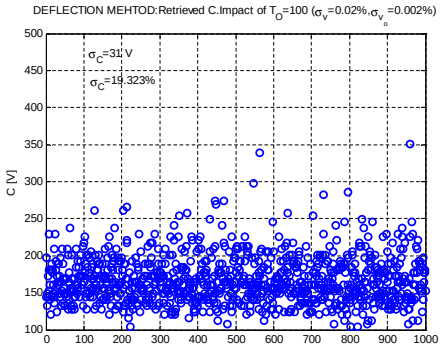

(b) Retrieved C parameter $T_O = 100\,K$

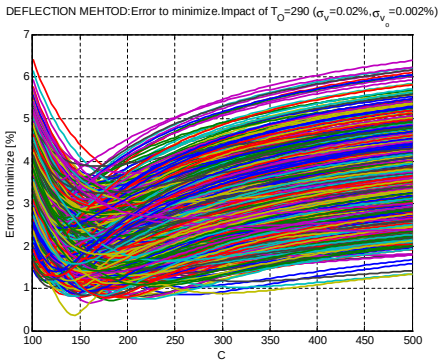

(c) Error to minimize $T_O = 290\,K$

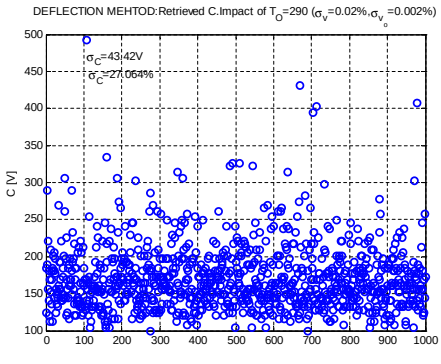

(d) Retrieved C parameter $T_O = 290\,K$

Figure 6.8: Impact of reference level in the characterization of non-linerarity by the Deflection method ($\sigma_{v_{A,AN}} = 0.02\%$, $\sigma_{v_{O,ON}} = 0.002\%$).

It can be seen that when the uncertainty of the reference level is reduced, the uncertainty of C is also reduced.

6.5 Conclusions

This section summarizes the main conclusions of this chapter.

A second method to characterize and correct non-linearities of the PMS has been presented. The deflection method is a more robust estimator of non-linearity when compared with the solpe method, basically because it does neither require the knowledge of the added noise nor the exact injected temperature at each level, and provides a quite simple non-linearity correction at voltage level.

The main sources of error in the measurement of C by the Deflection method depends on the uncertainty in PMS voltage reading (very sensitive). In order to characterize non-linearity by the Deflection Method, the non-linearity error should be higher than the noise, e.g.: if non-linearity error is about 0.2 %, the noise level in order to properly characterize this non-linearity should be below 0.02%.

In addition, it has been shown that a way to reduce the measurement uncertainty in C is by selecting a low reference level with a low uncertainty.

Chapter 7

Non linearity correction assesment

7.1 Introduction

This chapter is devoted to quantify the non-linearity error and to assess the impact of PMS linearity correction with relation to MIRAS amplitude calibration. Linearity correction is performed by the two procedures that have been presented in this thesis: Slope and Deflection methods. The impact of linearity correction is assessed by analyzing calibration data adquired in the Large Space Simulator (LSS) tests performed by EADS-CASA Espacio at ESA- ESTEC facilyties in Noordwijk during spring 2007. The following calibration parameters are analyzed:

1. Error on PMS Gain in percentage [%]
2. Error on PMS offset [mV]
3. Error on amplitude of FWF at origin $G_{kj}(0)$
4. Error on Tsys in measurement mode in percentage [%]

7.2 Impact of non linearity error in calibration parameters

This section analyzes the impact of linearity errors in the following calibration parameters: PMS Gain (G_{PMS}), PMS offset (v_{off}), amplitude of the Finge Washing Function (FWF) at origin ($G_{kj}(0)$) and System Temperature (T_{sys}).

The error on these magnitudes due to the non-linearity of the detector is evaluated by means of comparing these calibration parameters when no correction has been applied with the ones computed after applying the non-linearity correction, which is performed by the two procedures that have been presented in this thesis: Slope and Deflection methods. These calibration parameters are computed using the calibration data from LSS test, in particular IVT2 Stability Test 1 and Test PLM-DATA-PHASE-11-COLD-FUNCTIONAL, as input of the MIRAS-Testing Software developed by UPC, from now on MIRAS-TS. This software package fully processes SMOS data from level 0 up to Brightness Temeperature at antenna plane (level 1B) [24].

Hence in a general way, the relative error on parameter X due to the PMS non linearity can be computed as:

$$errorX\,[\%] = \frac{X^{(2)} - X^{(1)}}{X^{(1)}} \cdot 100 \tag{7.1}$$

and the absolute error can be computed as:

$$errorX = X^{(2)} - X^{(1)} \tag{7.2}$$

where the same nomenclature used in previous chapters is used in this section: superscript (1) indicates that no correction has been performed yet, and (2) indicates that the non linearity correction is already performed. On the other hand, $X^{(2)}$ is computed applying the two different correction methods that have been presented in this thesis: lope and Defelction Methods, following the procedures explained in sections 5.3 and 6.3 respectively.

7.2.1 Error on PMS Gain

Figure 7.1 shows the mean non-linearity error of all the calibrations performed during the test IVT2 Stability Test 1, for each of the 72 PMS receivers. The blue line represents the mean error of all receivers, which is around 0.8% for the slope method correction case and 0.81 % for the Deflection method. The standard deviation is 0.3% for the Slope Method and 0.29 % for the Deflection method. As it can be seen in the graphic, the non linearity error on PMS Gain presents a peak to peak dispersion of 1.6 % approximately for the slope method and 1.5% for the Deflection method.

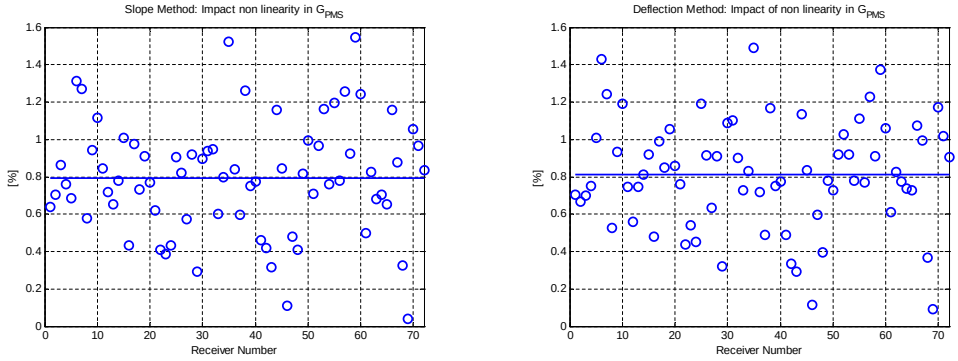

(a) Slope Method (b) Deflection Method

Figure 7.1: Impact of non linearity in G_{PMS}

Figure 7.2 shows for each receiver the maximum and minimum error of all the calibrations performed during the test, red and green points respectively, and the difference between the maximum and the minimum error has been represented in blue. As it can be seen in the graphic, the difference between maximum and minimum difference error is very low, below around 0.1% for the slope method, and even lower, arround 0.02%, for the deflection method.

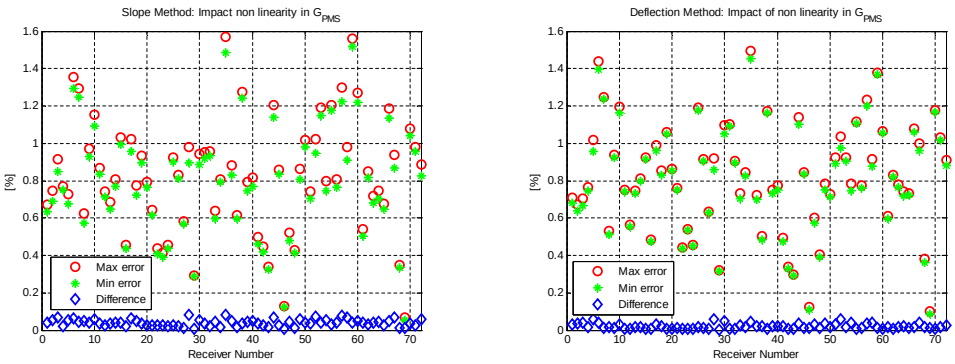

(a) Slope Method (b) Deflection Method

Figure 7.2: Impact of non linearity in G_{PMS} . The red points correspond to the maximum error of all calibrations, the green points to the minimum and the blue ones indicate the difference between maximum and minimum.

7.2.2 Error on PMS offset

This section shows the mean absolute non-linearity error on PMS offset for all the calibrations performed during the test IVT2 Stability Test 1. As it can be seen in Figure 7.3, both correction methods give a similar error on PMS offset.

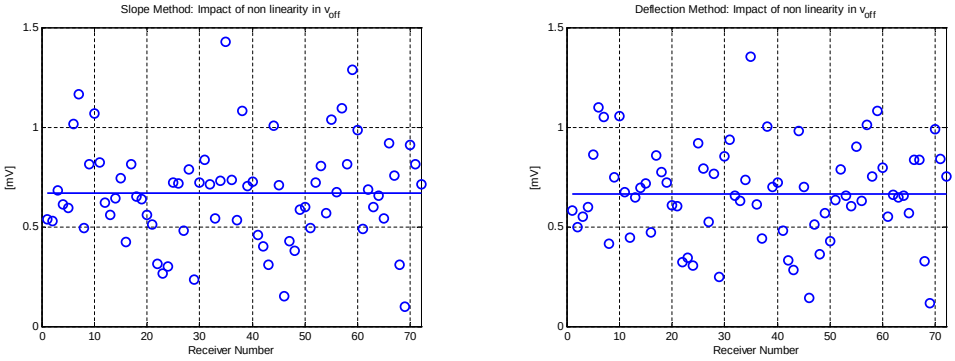

(a) Slope Method (b) Deflection Method

Figure 7.3: Impact of non linearity in v_{off}

7.2.3 Error FWF at origin

In a similar way than the previous sections, and for the same test (IVT2 Stability1 Test), the error on amplitude of FWF at origin has been evaluated. Figure 7.4 shows the mean non linearity error of all the calibrations performed during the test IVT2 Stability 1 Test, for each of the 2556 baselines. The mean error of all the baselines is represented in red, and it is around 0.22%.

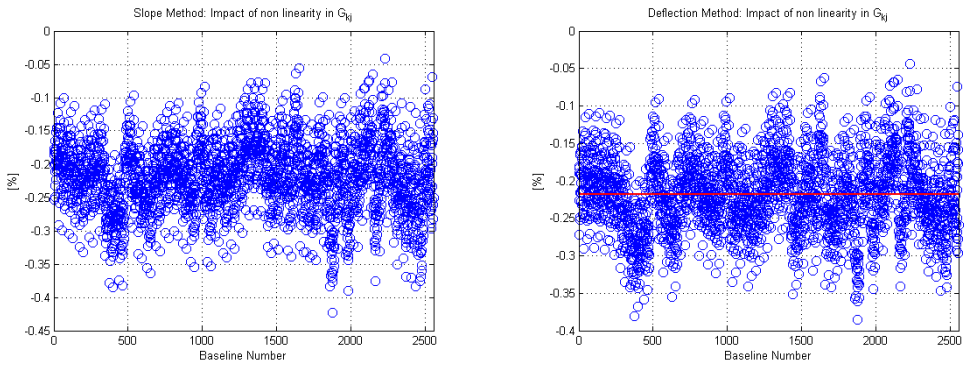

(a) Slope Method (b) Deflection Method

Figure 7.4: Impact of non linearity in G_{kj}

7.2.4 Error on Tsys

Figure 7.5 shows for each receiver the maximum and minimum error on system temperature of all the calibrations performed during the IVT2 Stability 1 Test, red and green points respectively, and the difference between the maximum and the minimum error has been represented in blue. As it can be seen in the graphic, the difference between maximum and minimum difference error is very low, below around 0.1% for the slope method, and even lower, arround 0.02%, for the deflection method. As it can be seen, this value is the same than the error on PMS gain. Therefore it can be conclude that the main non linearity error contribution to the system temperature non linearity error is due to the non linearity error on PMS gain.

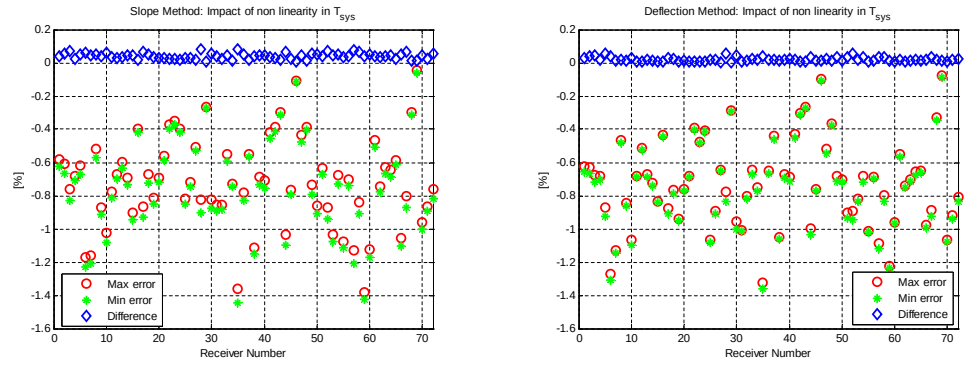

(a) Slope Method (b) Deflection Method

Figure 7.5: Impact of non linearity in T_{sys}: The red points correspond to the maximum error of all calibrations, the green points to the minimum and the blue ones indicate the difference between maximum and minimum.

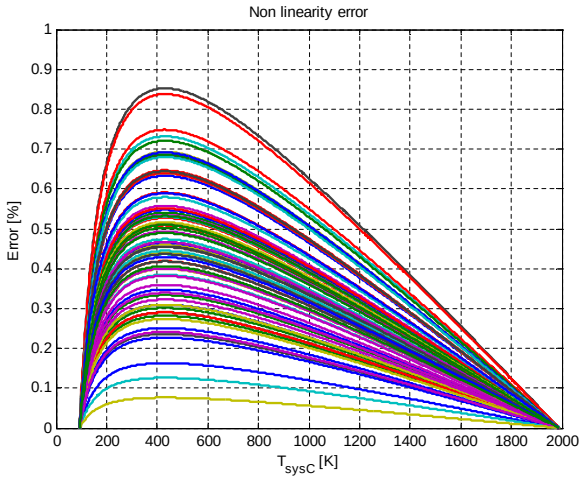

Figure 7.6: Non linearity error as function of system temperature

7.3 Non linearity error definition

This section shows and summarizes the non linearity error computed (at 21^{o}C) for all PMS receivers as defined in [21], which basically consists of the difference between the second order model with an ideal linear curve that joins the minimum and maximum system temperature points.

The main steps of the calculation of the non linearity error are summarized here after:

• Compute PMS second order model voltages as:

$$v_k = v_{off_k} + G_k T_{sys} + a_k T_{sys}^2 \tag{7.3}$$

Where v_{off_k}, G_k and a_k are available in the MIRAS Data Base (MDBfactory_v2xls) and T_{sys} is a 13,26 dB range [93.7K ,1990 K]

• Compute a linear curve that joins the minimum and maximum system temperature:

$$v_{ideal_k} = v_{off_{idealk}} + G_{idealk} T_{sys} \tag{7.4}$$

• The non linearity error [%] is defined as:

$$non\,linearity\,error\,[\%] = \frac{v_{ideal_k} - v_k}{G_{idealk} T_{sys}} \cdot 100 \tag{7.5}$$

Figure 7.6 shows the non linearity error as a function of T_{sys} for each of the 72 PMS receivers, computed following the procedure explained before. As it can be seen in Figure 7.6, all PMS receivers accomplish the requirement of non linearity error, which was set to 1%.

7.4 Residual non linearity error definition

This section is devoted to compute the residual non linearity error, after linearizing by the Deflection Method. For this purpose, a linearized second order model a_{lin} is estimated

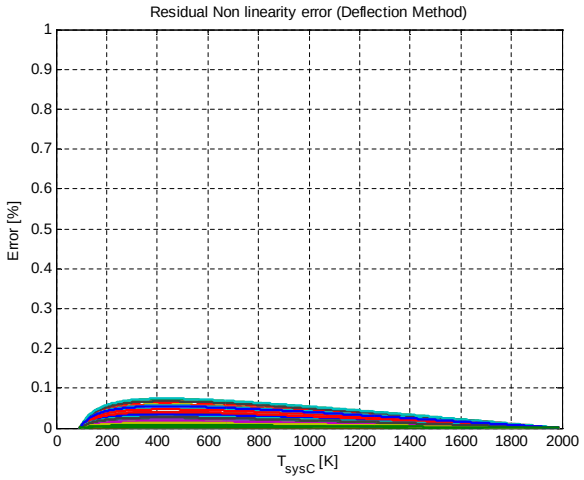

Figure 7.7: Non linearity error and residual non linearity error

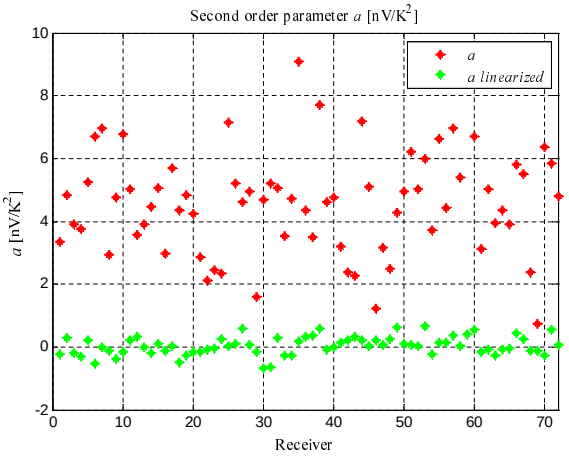

Figure 7.8: PMS non linearity term: before (red) and after (green) linearizing by the Deflection Method

by applying the Slope Method, after linearizing the data set available measured by Mier following the linearization procedure explained in section 6.3.

Figure 7.8 compares the second order parameter of both models before linearizing (red) and the one estimated after linearizing (green) all the PMS readings involved in the estimation by the Deflection linearization procedure detailed in section 6.3.

As it can be seen in Figure 7.8 the mean value of the second order parameter available in the MDB is about $4.51^{\mathrm{nV}/\mathrm{K}^2}$(red) and once the linearization procedure is applied, the mean of all the receivers after linearization is about 0.021 $^{\mathrm{nV}/\mathrm{K}^2}$ (green). That is, all the PMS have been linearized to the noise level.

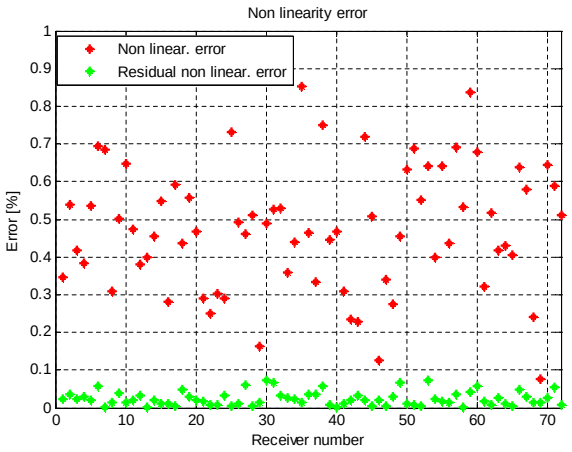

Figure 7.9: Non linearity error and residual non linearity error

Figure 7.9 shows the non-linearity error (red) and the residual non-linearity error (green) for all the 72 PMS. These values are computed as the maximum of Figures 7.6 and 7.7 respectivelly, for each receiver.

7.5 Evaluation of linearity correction by the consistency tool

The performance of the linearity correction by the Deflection method has been evaluated by means of the consistency tool [25], a key tool devoloped by the UPC Remote Sensing Group.

The rationale of the amplitude self-consistency tool is based on a quite simple principle: when all PMS in a section are fed by the same noise source, the difference in the system temperatures at their inputs between two noise injection levels (hot and warm) must be the same except for the Noise Distribution Network (NDN) unbalance. The remaining differences are an indicator of the cosistency of all the calibration procedure.

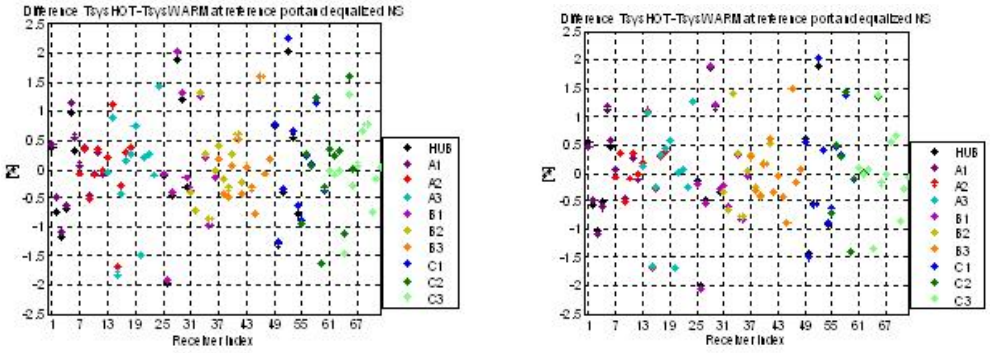

(a) Linearity correction is not performed (b) Linearity correction performed

Figure 7.10: Output of consistency tool

The output of the consistency tool for two different cases is shown in Figure 7.10:

• Figure 7.10a shows the output of consistency tool, when the S parameters amplitude correction has been calculated, without considering the linearity correction by the Deflection Method.

• Figure 7.10b shows the output of consistency tool, when the linearity error correction has been applied and the S parameters amplitude correction has been recalculated taking in to account the linearity correction by the Deflection method.

As it can be seen in the previous figures, the difference between the magnitude $T_{sysHOT} - T_{sysWARM}$ when receivers are fed by even and odd noise sources is lower when the linearity correction is applied (Figure 7.10b). This fact shows the correct performance of linearity correction by the Deflection method.

Although in almost all receivers, the difference $T_{sysHOT} - T_{sysWARM}$ when the receivers are fed by even and odd noise sources are more similar when the linearity correction is applied, the peak to peak dispersion is the same order of magnitude.

The total standard deviation in the difference $T_{sysHOT} - T_{sysWARM}$ (Figure 7.10a) ($\sigma_T = 0.82\%$) can be written as a contribution of the standard deviation in the S parameters and the PMS non linearity error:

$$\sigma_T = \sqrt{\sigma_{|S|}^2 + \sigma_{NL}^2} \tag{7.6}$$

When the linearity correction is performed, the standard deviation in the difference $T_{sysHOT} - T_{sysWARM}$ (Figure 7.10b) can be written as:

$$\sigma_T^{'} = \sqrt{\sigma_T^2 - \sigma_{NL}^2} = \sigma_{|S|} \tag{7.7}$$

In order to compute σ_{NL}, the difference between the magnitude $\Delta v = v_2 - v_1$ when no linearity correction is performed versus when it is performed ($\Delta v_{linearized}$) is shown in Figure 7.11.

Since PMS Gain is about 1 mV/K, it is assumed that the contribution of non linearity error in the standard deviation of the magnitude $T_{sysHOT} - T_{sysWARM}$ (Figure 7.10a) can be computed at a PMS voltage level (Figure 7.11). Hence $\sigma_{NL} = 0.2729\%$.

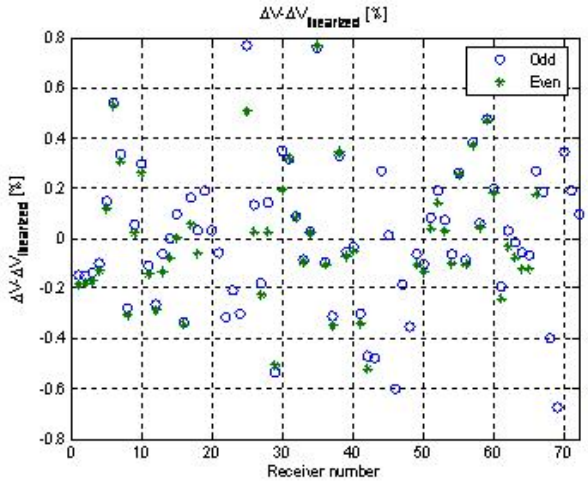

Figure 7.11: The difference between the magnitude $\Delta v = v_2 - v_1$ when no linearity correction is performed versus when it is performed ($\Delta v_{linearized}$)

Taking in to account that the error or uncertainty in the estimation of standard deviation of a set of 126 samples (Figure 7.10 and Figure 7.11) (72 odd+54 even) is about 6.3%, it can be shown the standard deviation of the non linearity error is in the range of the uncertainty of the estimation of :

$$\sigma_T^{'} = \sigma_T^{'} \pm 3\sigma_{\sigma_T^{'}} = [0.6341\%, 0.9124\%] \tag{7.8}$$

That is the reason why Figure 7.10a and Figure 7.10b have similar peak to peak dispersion.

Chapter 8

Conclusions

As main outcome of this thesis the non-linear error of the 72 PMS units in the MIRAS/SMOS instrument has been fully evaluated by means of both the so-called slope and the deflection methods. Both methods can be implemented with the same measurement set-up.

Deflection method is more robust than the slope method, basically because does neither require the knowledge of the added noise nor the exact system temperature at each level.

The main sources of error in the measurement of a by the Slope method depends on: systematic errors in the extra noise injected and the uncertainty in system temperature. On the other hand, the main sources of error in the measurement of C by the Deflection method depends on the uncertainty in PMS voltage reading (very sensitive). However it does not require neither the knowledge of the extra noise injected nor the system temperature.

In order to reduce the uncertainty in the measurement of C, a low reference level should be selected with low uncertainty. It can be achieved by taking and averaging more samples.

The main advantage of the linearization correction by the Deflection method is that it is a more simple procedure when compared with the linearization correction by the Slope Method, which requires one more iteration (estimation of T_{sys}) and provides a quite simple non-linearity correction at voltage level. In addition the correction paremeter C does not depend on the input plane, so it can be used to correct any PMS voltage. On the other hand, the slope method directly estimates the second order term, which is very useful to simulate the non-linearity error both in the PMS measurements and theoretical assessments.

After analyzing the results, the Deflection method is adopted as the technique to correct non-linearity of the PMS. The Deflection method has been implemented in the official SMOS Level-1 processor and the correction parameters C obtained during this thesis are included in the MIRAS Data Base, and will be used in the correction procedure. The consistency tool has been used to assess the correct performance of the non linearity correction by the Deflection method.

MIRAS/SMOS power detectors have shown a moderate non-linear error before correction in the range of 0.1% to 1% that has been reduced to a negligible residual non-linear error after correction by means of the Deflection method (below 0.1%).

Appendix A

Results

A.1 Communications to conferences

- **C.González-Haro**, F. Torres, N. Duffo, I. Corbella, sR. Vilaseca, P. de Paco, M. Martin-Neira. "Linearity Characterization of detectors for interferometric Radiomenters". Proc. IEE International Geoscience and Remote Sensing Sympossium IGARSS 2009, Cape Town South Africa. July 2009.

- F.Torres, V.Gonzalez-Gambau and **C.González-Haro**. "One-Point Calibration in Interferometric Radiometers Devoted to Earth Observation" Proc. SPIE Europe Remote Sensing 2008. Cardiff Wales, UK

- F.Torres, N.Duffo, **C.González-Haro**, R.Vilaseca, R.Sagues, M. Martin-Neira. "Assessment on Linearity Errors in Detectors for Interferometric Radiometers". Proc. IEEE International Geoscience and Remote Sensing Symposium (IGARSS 2008), Boston, MA, vol. 2, 7-11 July 2008, pp. II-1164-II1167.

A.2 Internal technical reports

- **C.González-Haro**, F.Torres, N.Duffo, I.Corbella, A.Camps and M.Vall-llosera. "PMS linearity correction assessment" SO-TN-UPC-PLM-0067, UPC, Tech. Rep., July 2008.

- **C.González-Haro**, F.Torres, N.Duffo, I.Corbella, A.Camps and M.Vall-llosera. "PMS linearity test set-up error analysis" SO-TN-UPC-PLM-0068, UPC, Tech. Rep., February 2009.

- **C.González-Haro**, F.Torres, N.Duffo, I.Corbella, A.Camps and M.Vall-llosera. "Estimation of second order correction by the Deflection Method" SO-TN-UPC-PLM-0078, UPC, Tech. Rep., February 2009.

- **C.González-Haro**, F.Torres, N.Duffo, I.Corbella, A.Camps and M.Vall-llosera. "Impact of reference level in the Deflection method estimation" SO-TN-UPC-PLM-0083 v1.1, UPC, Tech. Rep., May 2009.

- **C.González-Haro**, F.Torres, N.Duffo, I.Corbella, A.Camps and M.Vall-llosera. "Non linearity error correction by Deflection Method" SO-TN-UPC-PLM-0087, UPC, Tech. Rep., July 2009.
- **C.González-Haro**, F.Torres, N.Duffo, I.Corbella, A.Camps and M.Vall-llosera. "Impact of linearity correction by Deflection method" SO-TN-UPC-PLM-0079, UPC, Tech. Rep., October 2009.
- **C.González-Haro**, F.Torres, N.Duffo, I.Corbella, A.Camps and M.Vall-llosera. "Deflection Testing Software User Guide" SO-TN-UPC-PLM-0090, UPC, Tech. Rep., November 2009.

Bibliography

[1] Y.Kerr P.Silvestrin, M.Berger and J.Font. Esa's second earth explorer opportunity mission: The soil moisture and ocean salinity mission-smos. *IEEE Geosciene and Remote Sensing Newsletter*, 118:11–14, 2001.

[2] Y. H. Kerr, P. Waldteufel, J. P. Wigneron, J. Martinuzzi, J. Font, and M. Berger. Soil moisture retrieval from space: the soil moisture and ocean salinity (smos) mission. 39(8):1729–1735, Aug. 2001.

[3] J. Font, G. S. E. Lagerloef, D. M. Le Vine, A. Camps, and O. Z. Zanife. The determination of surface salinity with the european smos space mission. 42(10):2196–2205, Oct. 2004.

[4] Jodi Font Michael Berger Mark Drinkwater, Yann Kerr. Exploring the water cycle of the 'blue planet'. *ESA Bulletin*, 137:6–15, February 2009.

[5] M. Martin-Neira, Y. Menard, J. M. Goutoule, and U. Kraft. Miras, a two-dimensional aperture synthesis radiometer. In *Proc. International Geoscience and Remote Sensing Symposium IGARSS '94. Surface and Atmospheric Remote Sensing: Technologies, Data Analysis and Interpretation*, volume 3, pages 1323–1325, 8–12 Aug. 1994.

[6] K. D. McMullan, M. A. Brown, M. Martin-Neira, W. Rits, S. Ekholm, J. Marti, and J. Lemanczyk. Smos: The payload. 46(3):594–605, March 2008.

[7] I. Corbella, F. Torres, A. Camps, J. Bara, N. Duffo, and M. Vall-Ilossera. L-band aperture synthesis radiometry: hardware requirements and system performance. In *Proc. IEEE 2000 International Geoscience and Remote Sensing Symposium IGARSS 2000*, volume 7, pages 2975–2977, 24–28 July 2000.

[8] I. Corbella, N. Duffo, M. Vall-llossera, A. Camps, and F. Torres. The visibility function in interferometric aperture synthesis radiometry. 42(8):1677–1682, Aug. 2004.

[9] I. Corbella, F. Torres, A. Camps, A. Colliander, M. Martin-Neira, S. Ribo, K. Rautiainen, N. Duffo, and M. Vall-llossera. Miras end-to-end calibration: application to smos l1 processor. 43(5):1126–1134, May 2005.

[10] F. Torres, A. Camps, J. Bara, I. Corbella, and R. Ferrero. On-board phase and modulus calibration of large aperture synthesis radiometers: study applied to miras. 34(4):1000–1009, July 1996.

[11] J. Lemmetyinen, J. Uusitalo, J. Kainulainen, K. Rautiainen, N. Fabritius, M. Levander, V. Kangas, H. Greus, J. Pihlflyckt, A. Kontu, S. Kemppainen, A. Colliander, M. T. Hallikainen, and J. Lahtinen. Smos calibration subsystem. 45(11):3691–3700, Nov. 2007.

[12] A. Colliander, L. Ruokokoski, J. Suomela, K. Veijola, J. Kettunen, V. Kangas, A. Aalto, M. Levander, H. Greus, M. T. Hallikainen, and J. Lahtinen. Development and calibration of smos reference radiometer. 45(7):1967–1977, July 2007.

[13] F. Torres, I. Corbella, A. Camps, N. Duffo, M. Vall-llossera, S. Beraza, C. Gutierrez, and M. Martin-Neira. Denormalization of visibilities for in-orbit calibration of interferometric radiometers. 44(10):2679–2686, Oct. 2006.

[14] I. Corbella, F. Torres, N. Duffo, A. Camps, M. Vall-Ilossera, and V. Gonzalez. Miras in-orbit calibration. In *Proc. IEEE International Geoscience and Remote Sensing Symposium IGARSS 2007*, pages 3622–3625, 23–28 July 2007.

[15] P.Piironen. Pms offset determination using an if attenuator. Technical Report 14629/00/NL/SF, ESA-ESTEC, Holland, The Netherlands, June 2002.

[16] J. Capdevila I. Corbella F. Torres J. Bará, A. Camps. Miras calibration system definition and interference analysis (cas-d). Technical Report Final report, UPC, May 1998.

[17] F. Torres, N. Duffo, I. Corbella, A. Camps, M. Vallllossera, and L. Sagues. Dynamic range and linearity trade-off in detectors for. *Electronics Letters*, 39(25):1852–1854, 11 Dec. 2003.

[18] Online: http://www.mier.es/.

[19] N. Skou. Microwave radiometer linearity measured by simple means. In *Proc. IEEE International Geoscience and Remote Sensing Symposium IGARSS '02*, volume 6, pages 3664–3667, 24–28 June 2002.

[20] V. S. Reinhardt, Y. C. Shih, P. A. Toth, S. C. Reynolds, and A. L. Berman. Methods for measuring the power linearity of microwave detectors for radiometric applications. In *Proc. IEEE MTT-S International Microwave Symposium Digest*, pages 1477–1480, 23–27 May 1994.

[21] L.Sagués R. Vilaseca, M.Segarra. Pms linearity setup improvement. Technical Report SO-RP-MIER-LIC-0233, Mier Comunicaciones, February 2005.

[22] N. Duffo I.Corbella A.Camps C.González-Haro, F.Torres and M.Vall·llosera. Estimation of second order correction by the deflection method. Technical Report SO-TN-UPC-PLM-0078, UPC, February 2009.

[23] Fernando Pellerano William Wilson, Alan Tanner and Kevin Horgan. Ultra stable microwave radiometers for future sea surface salinity missions. Technical Report JPL Report D-31794, bJet Propulsion Laboratory, California Institute of Technology, Pasadena, California 91109 USA, April 2005.

[24] I. Corbella, F. Torres, N. Duffo, V. Gonzalez, A. Camps, and M. Vall-llossera. Fast processing tool for smos data. In *Proc. IEEE International Geoscience and Remote Sensing Symposium IGARSS 2008*, volume 2, pages II–1152–II–1155, 7–11 July 2008.

[25] V. Gonzalez-Gambau, F. Torres, N. Duffo, and M. Martin-Neira. Calibration consistency tool for interferometric radiometers. In *Proc. IEEE International Geoscience and Remote Sensing Symposium IGARSS 2008*, volume 5, pages V–401–V–404, 7–11 July 2008.